공학박사 학위논문

Atmospheric-pressure plasma treatment toward high-quality solution-processed metal oxide films in thin-film transistors

대기 플라즈마 처리를 통한 고성능 용액 공정 금속 산화물 박막 트랜지스터 개발에 관한 연구

2020년 8월

서울대학교 융합과학기술대학원

융합과학부 나노융합전공

박 진 택

Atmospheric-pressure plasma treatment toward high-quality solution-processed metal oxide films in thin-film transistors

지도교수 김 연 상

이 논문을 공학박사학위 논문으로 제출함

2020년 7월

서울대학교 융합과학기술대학원
융합과학부 나노융합전공

박 진 택

박진택의 박사학위 논문을 인준함

2020 년 6 월

위 원 장	박 원 철	인
부위원장	김 연 상	인
위 원	이 강 원	인
위 원	강 성 준	인
위 원	김 주 형	인

Abstract

Atmospheric-pressure plasma treatment toward high-quality solution-processed metal oxide films in thin-film transistors

Jintaek Park

Program in Nano Science and Technology

The Graduate School of Convergence Science & Technology

Seoul National University

Solution-process have drawn considerable attention as a thin-film deposition method for thin-film transistor (TFT), because they do not require cumbersome equipment compared to the vacuum process such as radio frequency magnetron sputtering, atomic layer deposition and pulsed laser deposition. Therefore, oxide semiconductors and oxide dielectrics using solution-process method have been studied in a simple and inexpensive process. However, the application of solution-processed TFTs to the industry is still difficult because of the insufficient electrical properties as compared with a vacuum-processed thin film. Thus, many researches have been conducted to improve the properties of solution-processed thin films.

Among them, conventional plasma treatment in vacuum conditions has been studied since oxygen plasma treatment controls the oxygen vacancy. Unfortunately, introduction of the vacuum treatment makes it difficult to apply the plasma treatment to the solution-treated thin film because the advantage of the solution process is lost. Accordingly, there is a growing demand for a technique suitable for application to solution-treated thin films in an industrial field.

Herein, I present an atmospheric-pressure plasma (APP) treatment technique for improving the electrical performance of solution-processed films. Firstly, I have implemented improvements in important TFT parameters, V_{on} and the on/off current ratio, which still keep up the high field-effect mobility, by introducing the APP treatment into solution-processed InO_x TFTs. Secondly, AlO_x dielectric film using aqueous route method was deposited by a solution process and its characteristics were improved. Characteristic changes through APP treatment were observed by measurement of capacitance-frequency and breakdown voltage. It was observed that the breakdown voltage of AlO_x thin film was increased by APP treatment. To investigate the changes of binding relationship according to APP treatment time, X-ray photoelectron spectroscopy (XPS) was performed. TFTs were fabricated by depositing a solution-processed InO_x with a semiconductor film, and the characteristics were evaluated. The field-effect mobility was increased compared to the untreated samples. Thin-film deposition including semiconductor and gate dielectric and plasma treatment were performed

in a non-vacuum environment. The process temperature was below 250 ℃.

In summary, I introduce the potential of APP treatment that can simply control the carrier concentration of solution-processed OS thin film and improve the breakdown voltage of solution-processed gate dielectric thin film. This APP technique can provide advances toward industrial applications of solution-processed TFTs, while maintaining the advantages of the solution process.

Keywords: Atmospheric-pressure plasma, oxide semiconductor, gate dielectric, thin-film transistor, solution process, low temperature process

Student Number: 2016-39007

Contents

List of figures and tables

Chapter 1

Chapter 2

Chapter 3

Abbreviations

TFT Thin-film transistor

LTPS Low temperature poly silicon

XPS X-ray photoelectron spectroscopy

AFM Atomic force microscopy

UV Ultraviolet

LCD Liquid crystal display

a-Si:H hydrogenated amorphous silicon

OLED Organic light emitting display

MOSFET Metal oxide semiconductor field-effect transistor

V_{th} Threshold voltage

V_{gs} Gate-source voltage

I_{ds} Drain-source voltage

V_{ds} Drain-source voltage

μ Field-effect mobility

SS Subthreshold swing

V_{on} Turn-on voltage

IGZO Indium gallium zinc oxide

CBM Conduction band minimum

VBM Valence band maximum

OS Oxide semiconductor

RC Resistance-capacitance

ALD Atomic layer deposition

PLD Pulsed laser deposition

SEM Scanning electron microscopy

O_{vac} Oxygen vacancy

M-O Metal-oxide

APP atmospheric-pressure plasma

E_a activation energy

MIM Metal-insulator-metal

MISM Metal-insulator-semiconductor-metal

g_m Trans-conductance

N_{max} maximum trapped charge density

Chapter 1

Introduction

1.1 Overview

Thin-film transistors (TFTs) used as switching devices in the display industry are generally fabricated by depositing electrodes, dielectrics, and semiconductor materials onto substrates such as Si wafer, glass, or flexible films. [1-3] These thin films are successfully deposited in a vacuum atmosphere using various methods including radio frequency magnetron sputtering, atomic layer deposition and pulsed laser deposition. Nevertheless, the vacuum equipment is cumbersome, expensive, and difficult to fabricate in large scale, simple and cheap solution process techniques such as combustion, spray pyrolysis, ink-jet, and spin coating and have been mounting interest as thin film depo sition methods. Among them, an aqueous route method capable of depositing a high-quality thin film at a relatively low temperature (~ 300 ℃) by a simple process has been actively studied. [4,5] The aqueous route method has realized solution-processed indium oxide (InO_x) TFTs with a remarkably high field-effect mobility (> 10 cm^2/Vs) despite being fabricated with a low temperature (< 300 °C) process, which has shown new possibilities for practical application of solution-processed OS TFTs. However, despite the excellent electrical properties with high field-effect mobility, the application of a solution-processed OS TFTs still remains a difficult task as a practical technology due to the major disadvantages of current ratio. In conventional display technology, the V_{on} and

on/off current ratio are as important as the field-effect mobility of the TFT because they are strongly related to power consumption of the device in practical industrial application. The V_{on} and on/off current ratio of TFT are determined in consideration of various factors such as thickness, trap density, gate metal type and carrier concentration of a semiconductor. Among them, in practical TFT applications, the V_{on} and the on/off current ratio are mainly controlled by the carrier concentration of a semiconductor. For this reason, the control of carrier concentration of semiconductor is essential for the practical application of solution-processed OS TFTs.

To address this issue, this dissertation focuses on the development of atmospheric-pressure plasma treatment toward high-quality solution-processed oxide films in thin-film transistors. Before addressing the issues, basic concepts of TFTs and background are provided in chapter 1.

In chapter 2, I propose an effective atmospheric-pressure plasma (APP) treatment for simple and effective control of the carrier concentrations and important TFT parameters of solution-processed OS TFTs, such as V_{on} and on/off current ratio. I have successfully implemented the improvements in important TFT parameters, V_{on} from -11.4 V to -1.9 V and the on/off current ratio from ~10^3 to ~10^6, which still keep up the high field-effect mobility (> 20 cm^2/Vs), by introducing the APP treatment into solution-processed InO_x TFTs fabricated at low temperature condition (~ 250 °C). Based on various analyses

such as X-ray photoelectron spectroscopy (XPS), electrical characterization, and UV-Visible spectroscopy, I identified that the APP treatment can effectively control oxygen vacancy and carrier concentration in solution-processed OS. These results show that the APP treatment has a great potential for significantly modulating the electrical properties of solution-processed OS TFTs. This work has been published as "Effective Atmospheric-Pressure Plasma Treatment toward High-Performance Solution-Processed Oxide Thin-Film Transistors" by J. Park, J.-E. Huh, S.-E. Lee, J. Lee, W. H. Lee, K.-H. Lim and Y. S. Kim, ACS Appl. Mater. Interfaces, 10, 30581-30586 (2018). [6]

In chapter 3, I propose an APP post-treatment technique that can effectively improve the electrical properties of the AlO_x dielectric film deposited by a solution process using the aqueous route method. Characteristic changes through the APP treatment were observed by a measurement of capacitance-frequency and leakage current. The frequency dependency of AlO_x capacitance was reduced by the APP treatment. Also, as the APP treatment time increased, the leakage current density decreased. The root-mean-square surface roughness of all samples investigated by atomic force microscopy (AFM) is in the range of 0.12–0.16 nm and maintains an ultra-smooth surface regardless of the APP treatment. The changes of binding a relationship according to the APP treatment time were analyzed by x-ray photoelectron spectroscopy (XPS). Through the APP treatment, the aluminum oxide ratio of the AlO_x dielectric films was

increased while the aluminum hydroxide ratio was decreased. Finally, TFTs including solution-processed AlO_x dielectric films were fabricated by depositing a solution-processed InO_x as a semiconductor film, and the characteristics were evaluated. The field-effect mobility of TFTs was increased from 9.77 to 26.79 $cm^2\ V^{-1}\ s^{-1}$ due to the effect of the APP treatment on solution-processed AlO_x dielectric thin films. Moreover, for the APP-treated samples, the mobility remained constant over a wide frequency operating range. These results are valuable as a way to effectively improve the electrical characteristics of the dielectric thin film, which is an essential component of the TFTs, with a low temperature process condition while maintaining the advantages of the solution process. This work has been published as "Atmospheric-Pressure Plasma Treatment toward High-Quality Solution-Processed Aluminum Oxide Gate Dielectric films in Thin-Film Transistors" by J. Park, N.-K. Cho, S.-E. Lee, E. G. Lee, J. Lee, C. Im, H.-J. Na and Y. S. Kim, Nanotechnology, 30, 495702 (2019) and "Investigation of Vertical Current Phenomena in the Insulator/Oxide Semiconductor Heterojunction Using XPS Analysis and an Atmospheric-Pressure Plasma Treatment System" by N.-K. Cho, J. Park, D. Lee, J.W. Park, W. H. Lee and Y. S. Kim, ACS Appl. Elect. Materilas, 1, 1698-1704 (2019). [7,8]

Finally, in chapter 4, the overall conclusion of this dissertation are summarized.

1.2 Thin-film transistors: Structures and parameters

Thin-film transistors (TFTs) are three terminal devices consist of semiconductor, gate insulator and electrodes, which are normally used as switching devices in liquid crystal display and organic light emitting display. Due to the simple structure and functionality of TFTs for large area applications on a variety of substrates from glass to flexible plastics, TFTs have been used in numerous electronic devices including transparent and flexible displays, memory devices, and sensors. [9-11] For application to next generation devices, TFTs require high performance and low power operation. However, despite such advantages, in the fabrication process of TFTs using the solution process, it is a fatal problem that there are hardly any ways to simply and effectively control important TFT parameters, including the turn-on voltage (V_{on}) and on/off current ratio. Since semiconductor and gate insulators are essential for TFT operation, many researchers have tried to improve the performance of TFTs by improving these thin films. [12,13]

The structures of TFTs are divided into four types according to the position of the gate electrode and to the distribution of the electrodes relatively to the semiconductor. [14,15] (Figure 1.1) Each structure is determined by the chracteristics of the semiconductor and fabrication conditions. For example, the bottom gate structure is widely used in liquid crystal display (LCD). This is

because the bottom gate shield the photosensitive armorphous silicon (a-Si:H) from the influence of the backlights present on LCD. On the other hand, the top gate structure is used when the semiconductor material requires a high temperature that could degrade the other layers previously deposited. So, the top gate structure is used for OLED applying the poly silicon TFT. Therefore, the structure of the TFT should be determined taking into account the properties of each component layer and interface to achieve the desired performance.

TFTs are similar to other field-effect devices in terms of operation and composing layers, such as MOSFETs. However, there are some differences between TFTs and MOSFETs. In the view of operaion mechanism, in TFTs the conductance of the semiconductor close to its interface with the insulator is achived by an accumulation layer, while in MOSFETs an inversion region has to be formed close to that interface. [14,15]

Ideal operation of n-type metal oxide semiconductor TFTs is explained as follows. [16] With the source grounded, a positive voltage is applied to the drain to pull electrons from the source to the drain electrode. The amount of drain current (I_{ds}) flowing from the source to the drain electrode depends on whether the electron accumulation layer exists at the metal-insulator interface. When a gate voltage (V_{gs}) is greater than V_{on} while V_{ds} is positive, drain current flows. As I mentioned above, to operate the TFT, the gate voltage (V_{gs}) and drain voltage (V_{ds}) must apply to each electrode. Dielectric layer is inserted between

semiconductor and gate electrode as a gate insulator, which induced charges at the interface between semiconductor and dielectric layer by modulating gate bias. In the case of n-type semiconductor-based TFT, below the threshold voltage (V_{th}), a depletion layer is formed near the interface of the gate insulator and semiconductor layer, meaning that it is in an off-state with few moving charge carriers. When the gate-source voltage (V_{gs}) is less than the threshold voltage (V_{th}), the drain current does not flows because carriers are not sufficient in the channel. (Figure 1.2, 1.3) On the other hand, when a positive gate voltage higher than V_{th} is applied (V_{gs}> V_{th}), charge carriers accumulate at the interface. Electrons are injected from the source into the gate bias induced electron accumulation layer channel, are transported across this low resistance accumulation layer, and are extracted at the drain electrode. The magnitude of drain current depends on the gate overvoltage, that determines the accumulation layer sheet charge density, and also on the magnitude of the drain voltage, which establisheds the electric field aided drift condition along the channel. [16] In the case of V_{gs}-V_{th} >>V_{ds} , drain current flow in the channel is explained by Ohm's law.

At this time, depending on the positive drain voltage (V_{ds}), I_{ds} behavior divided into linear region and saturation region, respectively. (Figure 1.2, 1.3)

- Linear region : V_{gs} - V_{th} > V_{ds}

$$I_{ds,lin} = \frac{W}{L} C\mu_{lin}\left(\left(V_{gs} - V_{th}\right)V_{ds} - \frac{V_{ds}^2}{2}\right) \qquad (1)$$

- Saturation region : V_{gs} - V_{th} < V_{ds}

$$I_{ds,sat} = \frac{W}{2L} C \mu_{sat} (V_{gs} - V_{th})^2 \qquad (2)$$

where W/L is the channel width and length, C is the capacitance of the dielectric layer. μ_{lin} and μ_{sat} are field-effect mobility in linear and saturation region, respectively.

The electrical characteristics of TFTs which determine device performance are evaluated in terms of several parameters such as on/off current ratio, field effect mobility, turn-on voltage, and subthreshold swing.

- On/off current ratio

On/off current ratio is defined as the ratio of the maxium and minimum values of the drain current.

- Field-effect mobility

Field-effect mobility can be obtained by equation 1 and 2.

$$\mu_{lin} = \frac{L}{WCV_{ds}} \frac{\partial I_{ds}}{\partial V_{gs}} \qquad (3)$$

$$\mu_{sat} = \frac{2L}{WC} \left(\frac{\partial \sqrt{I_{ds}}}{\partial V_{gs}} \right)^2 \qquad (4)$$

- Subthreshold swing (SS)

Subthreshold swing represent V_{gs} required to increase I_{ds} by 10 times in the

subthreshold reqion.

$$SS = \frac{\partial V_{gs}}{\partial (log_{10} I_{ds})} \quad (5)$$

- Threshold voltage (V_{th})

Threshold voltage means the minimum gate voltage to induce the channel layer in semiconductor. The V_{th} value can be obtained by linear extrapolation of the $I_{ds}^{1/2}$-V_{gs} plot.

- Turn on voltage (V_{on})

Turn on voltage indicates V_{gs} at which I_{ds} begins to increase.

As the applied positive drain voltage increases, if V_{ds} is not negligibly small compared to the overvoltage, drain current no longer has ohmic characteristics with respect to V_{ds} and the channel pinch-off occurs. (Figure 1.3) [16]

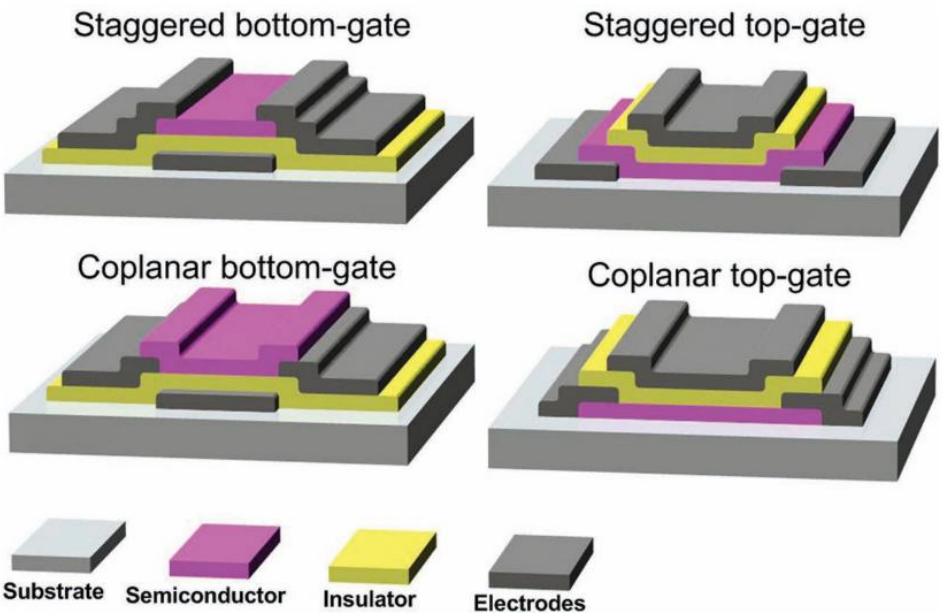

Figure 1. 1 The typical structures of TFTs. [14]

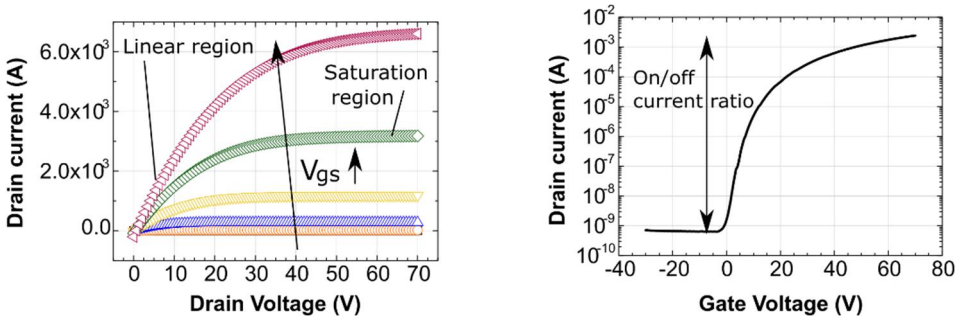

Figure 1. 2 Output and transfer characteristics of TFTs.

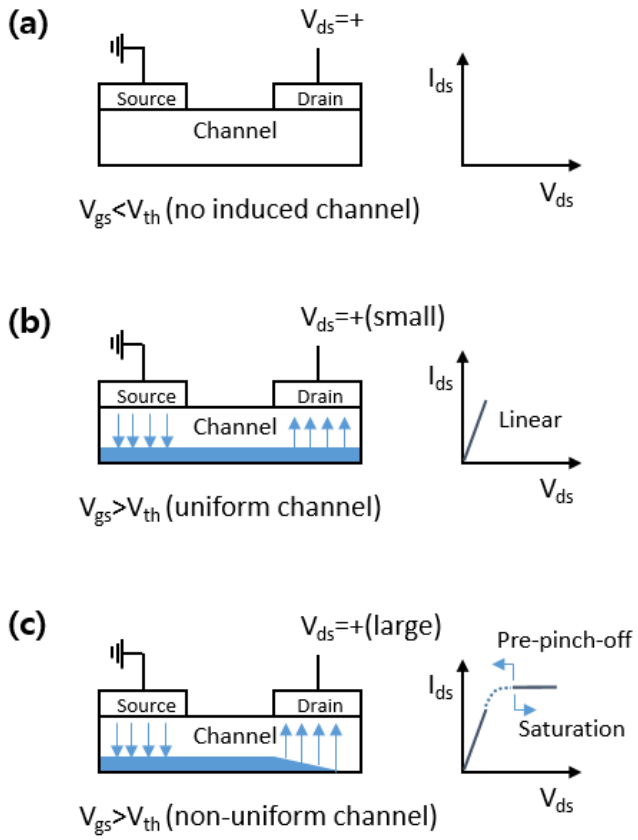

Figure 1. 3 Ideal n-type TFT operation. (a) Cut-off. (b) Linear, pre-pinch off. (C) Nonlinear, pre-pinch-off and post-pinch-off, saturation. [16]

1.3 Oxide semiconductor for TFT

Metal oxide semiconductors have attracted great attention as a promising switching device because they can quickly and simply produce transparent channels on flexible substrates with the advantages of low temperature precess, large area deposition, low cost and high mobility. In current display industry, Si-based TFTs such as hydrogenated amorphous silicon (a-Si:H) and low temperature polycrystalline silicon (LTPS) have been widely used as switching device. However, hydrogenated amorphous silicon has relatively low mobility, making it unsuitable for advanced displays.[17-19] Therefore, LTPS and oxide semiconductor TFTs have been mounting interest as candidates to replace hydrogenated amorphous silicon. In the case of LTPS TFT, it manufactured with laser beam has high field-effect mobility of above 100 $cm^2\ V^{-1}s^{-1}$, but it is quite difficult to apply to large displays because it has non-uniform electrical properties in a large area. Moreover, this process requires cumbersome laser equipment and the LTPS has poor transparency, which serves a drawback for future display application. On the other hand, oxide semiconductor TFT has good electrical and unique properties such as high optical transparency and flexibility. [20-22]

Oxide semiconductors are regarded as ionic semiconductors, which compose of metal cation of In, Zn, and Ga, with electronic configurations of $(n-1)d^{10}ns^0$.

For amorphous metal oxide semiconductors, n should be greater than or equal to 5 to ensure ns orbital overlap. In silicon-base materials, the conduction band minimum (CBM) and valence band maximum (VBM) are created in the anti-bonding (sp^3 σ*) and bonding (sp^3 σ) states of the Si sp^3 hybrid orbital, and the band gap is formed by energy splitting of the level of σ * -σ (Figure 1.4a). In contrast, since oxide have strong ionicity, CBM and VBM are usually formed from different ionic species. When the metal atom and oxygen atom are away from each other in the vacuum, the energy level of the highest occupied atomic orbital is not significantly different, as shown in Figure 1.4b, and is stable in the neutral atom state. As they get closer, charge transfer occurs because the electron affinity is different. As described above, the neutral state is more stable in vacuum without interaction, but the ionized ions form a negative electrostatic potential at the cation site and a positive potential at the anion site (Madelung potential), resulting in stabilize the ionized state in the ionic material (Figure 1.4c). Madelung potential lowers the energy level of oxygen ions and increases the energy level of metal cations (Figure 1.4c). Thus, conduction band minimum in oxide semiconductor is mainly composed of a unoccupied s orbital of a metal cation and the valence band maximum by occupied O 2p orbitals, and thus exibits high mobility even in an amorphous structures. [23,24] (Figure 1.5) Accordingly, the oxide semiconductors can be manufactured at low temperature in a transparent state, which is an advantageous for applying various substrates.

Oxide semiconductor TFTs have been studied since 1962. At that time, TFT did not represent good electrical performances, In the early 2000s, there were studies that TFTs using ZnO, InZnO and InGaZnO showed excellent electrical properties regarding the application of amorphous multicomponent. After that oxide semiconductors have been focused by tons of researchers and various kinds of studies for properties of InGaZnO such as band gap state and chemical structures have been investigated. [25-27] (Figure 1.6) For instance, the M-O bonding is known to provide fast conduction pathways for carriers, while the meaning of V_o is complicated in forming various subgap states, as shown in Figure 1.7. C. Liu *et al.* reported that one oxygen vacancies have small vacancy sizes and form states near the conduction band minimum (type-I), and they do not trap electrons but provide free carriers, acting as shallow donor-like states. The other oxygen vacancies have large vacancy sizes and form deep trap levels far from the conduction band minimum (type-II), acting as deep donor-like states. [28-33] (Figure 1.8)

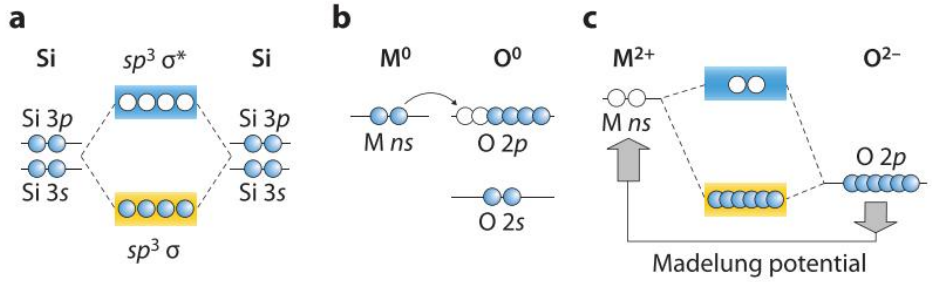

Figure 1. 4 Schematic electronic structures of silicon and ionic oxide semiconductors. [24]

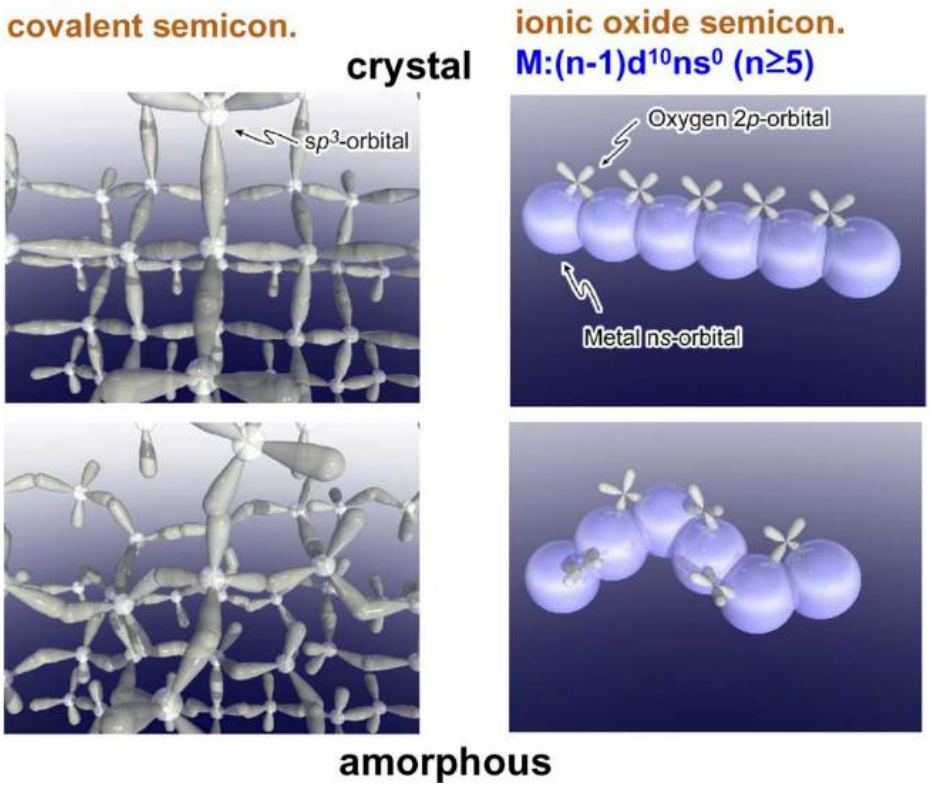

Figure 1. 5 Schematic orbital of electron pathway in conventional semiconductor and oxide semiconductor. [24]

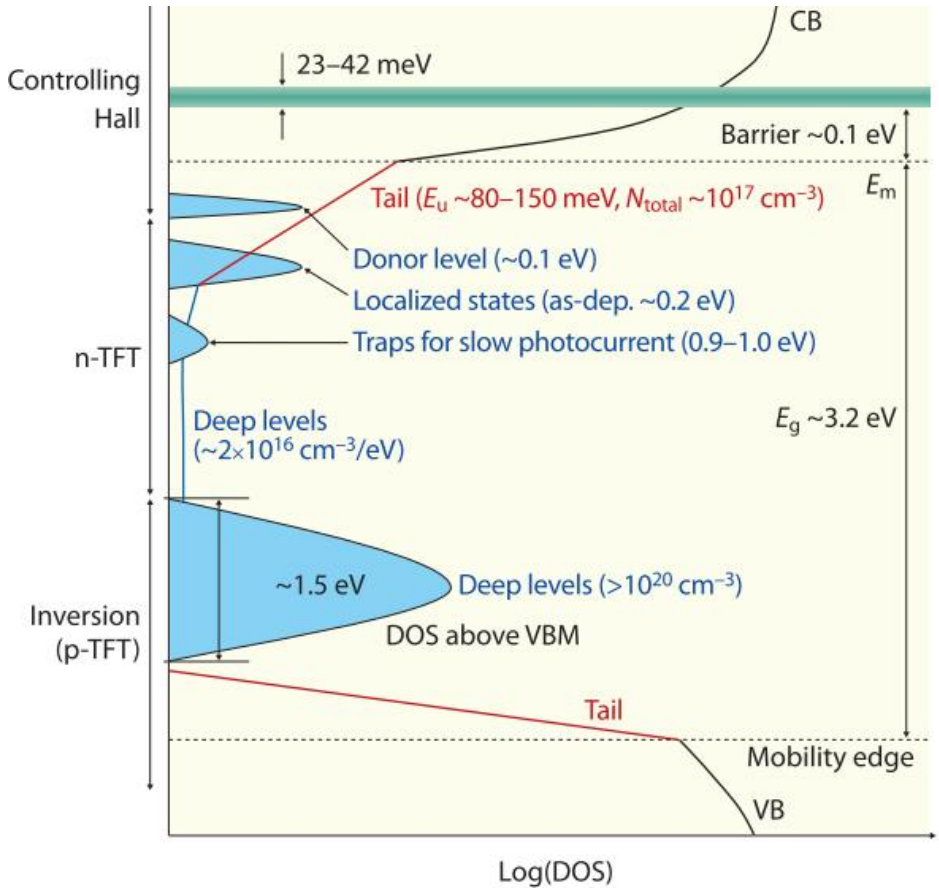

Figure 1. 6 Schematic electronic structure of amorphous IGZO. [27]

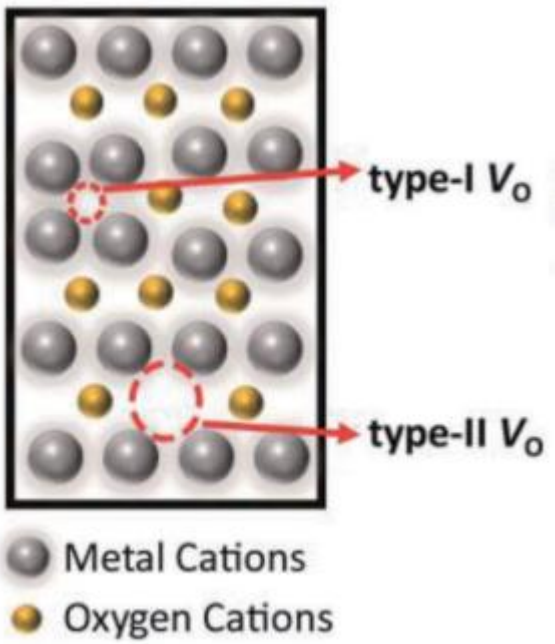

Figure 1. 7 Schematic representations for oxygen vacancy. [33]

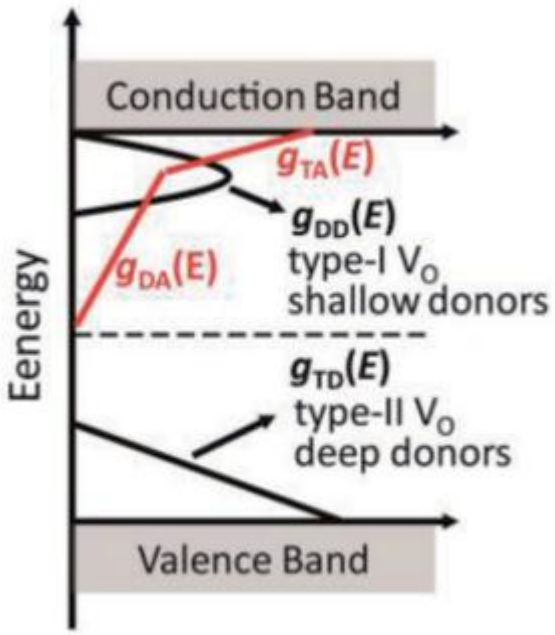

Figure 1. 8 Schematic representations for their contributions to the subgap states.

[33]

1.4 Solution-processed TFT

Unlike conventional fabrication which uses cumbersome and expensive vacuum equipments, solution process carried out by the coating and dropping of a solution to fabricate a oxide semiconductor layer. Also, since techniques such as inkjet printing and screen printing can be applied, a photolithography system is not necessary. In addition, a continuous manufacturing process is possible using a roll-to-roll process. Various methods of solution deposition were schematized in Figure 1.9. [34] Among them, a metal-organic deposition solutions can chemically react to build-up networks in solution through the sol-gel method. In the sol-gel processing, the precursor undergoes thermally driven hydrolysis (Figure 1.10) and condensation reactions in solution to produce a stable suspension of colloidal particles (a sol) and evolve towards a porous solid network in the liquid (a gel). The gelation process is linking metal centers with oxo (M-O-M) or hydroxo (M-OH-M) bridges through condensation reactions including alcohol or water elimination. (Figure 1.11) For example, as shown in Figure 1.12, the water replaces all the nitrate ions during solvation to form the hexaaqua indium(III) cation ($[In(H_2O)_6]^{3+}$) and InO_x film can be obtained through thermally driven condensation reactions. It is reported that the nitrate-baased solution provided the highest quality InO_x film at low temperature (250 °C) could showed the highest field-effect mobility as a TFT semiconductor

material. [35,36]

However, despite the advantages of solution process, the application of solution-processed oxide semiconductor TFTs still remains a difficult task as a practical technology due to their poor electrical characteristics compared with vacuum-processed oxide semiconductor TFTs.

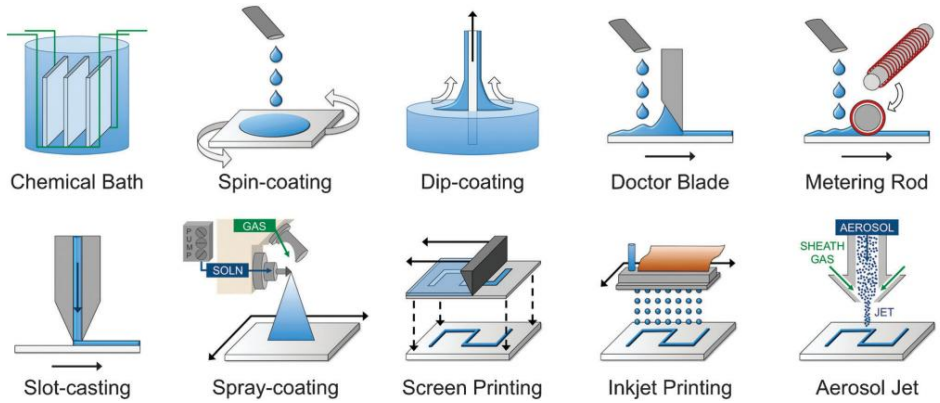

Figure 1. 9 Depiction of various solution deposition methods. [35]

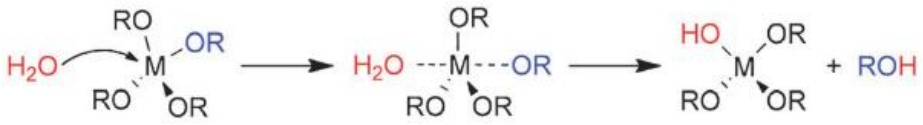

Figure 1. 10 Hydrolysis of metal alkoxide. [35]

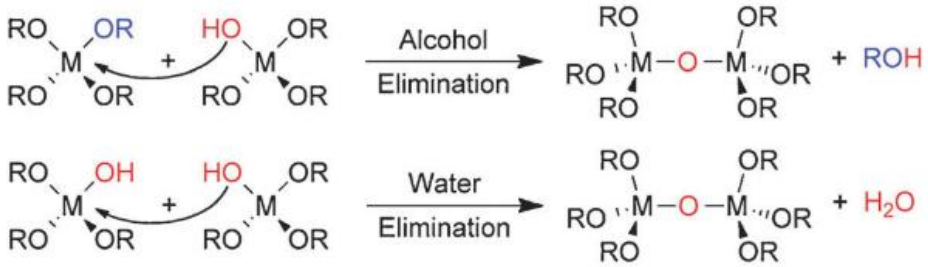

Figure 1. 11 Condensation can occur by elimination. [35]

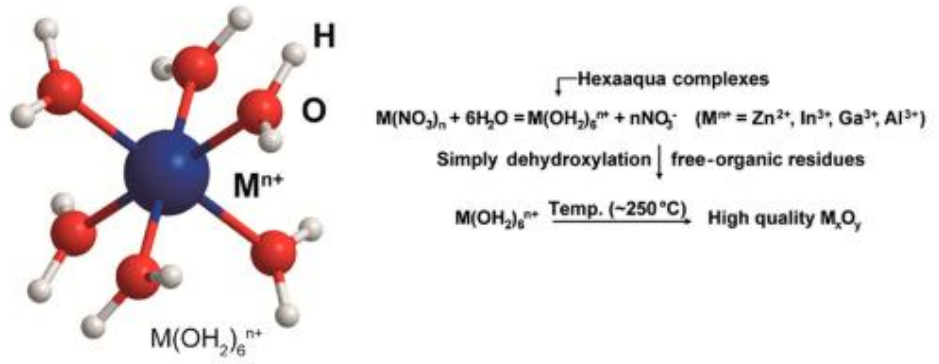

Figure 1. 12 Structure and processing of hexaaqua metal complexes.[36]

1.5 Dielectric engineering

The gate dielectric is an essential component of TFT in which insulating material separates the gate electrode and the semiconductor layer to induce a channel and prevent electrical shorts between the gate electrode and the semiconductor layer. To improve TFT performance, various materials such as organic, inorganic, and hybrid materials have been studied. Among them, SiO_2 has been widely used due to its excellent insulating properties and thermodynamic stability. [37-40] However, SiO_2 has an intrinsic limitation for the low charge carrier inducement in semiconductor layer by intrinsic low dielectric constant. In order to promote the potential of metal oxide TFTs general, high-k materials such as AlO_x,YO_x, TaO_x, HfO_x, and ZrO_x have been investigated as dielectric layers in TFTs because they can provide large gate capacitance without significantly increasing gate leakage current. [41-46] (Figure 1.13) In the case of solution-deposited oxide dielectrics induce poor electrical properties and stability than vacuum-deposited dielectrics in TFTs. Therefore, more research is needed on how to obtain a high-quality dielectric layer while maintaining the advantages of a solution process.

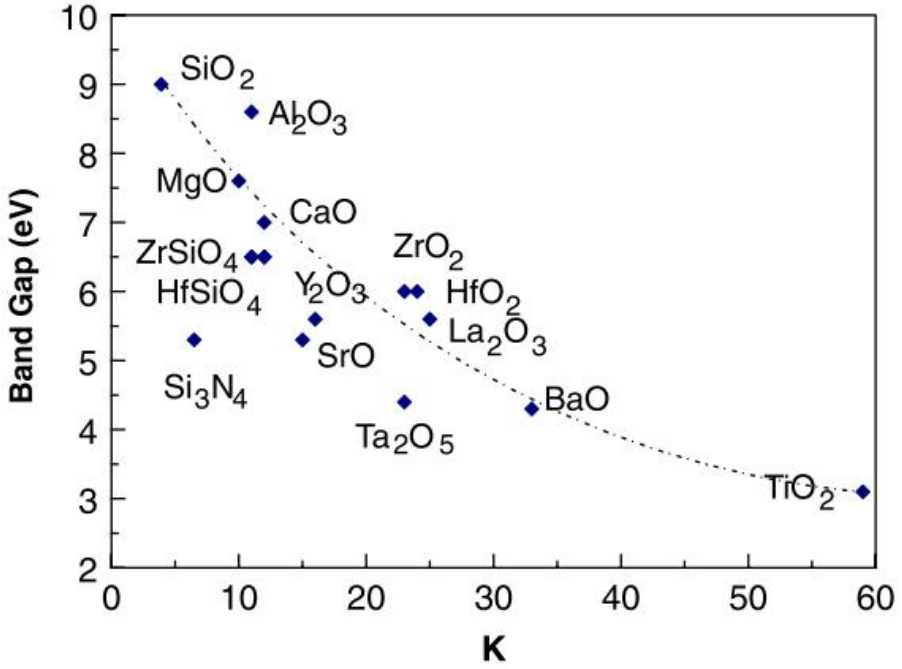

Figure 1. 13 Static dielectric constant vs. band gap for candidate gate oxide. [42]

1.6 References

[1] E. Fortunato, P. Barquinha, and R. Martins, Adv. Mater. **24**, 2945 (2012).

[2] P.K. Nayak, Z. Wang, and H.N. Alshareef, Adv. Mater. **28**, 7736 (2016).

[3] S.Y. Park, B.J. Kim, K. Kim, M.S. Kang, K.H. Lim, T. Il Lee, J.M. Myoung, H.K. Baik, J.H. Cho, and Y.S. Kim, Adv. Mater. **24**, 834 (2012).

[4] Y. Hwan Hwang, J.-S. Seo, J. Moon Yun, H. Park, S. Yang, S.-H. Ko Park, and B.-S. Bae, NPG Asia Mater. **5**, e45 (2013).

[5] K.-H. Lim, J. Lee, J.-E. Huh, J. Park, J.-H. Lee, S.-E. Lee, and Y.S. Kim, J. Mater. Chem. C **5**, 7768 (2017).

[6] J. Park, J.E. Huh, S.E. Lee, J. Lee, W.H. Lee, K.H. Lim, and Y.S. Kim, ACS Appl. Mater. Interfaces **10**, 30581 (2018).

[7] J. Park, N.-K. Cho, S.-E. Lee, E.G. Lee, J. Lee, C. Im, H. Na, and Y.S. Kim, Nanotechnology **30**, 495702 (2019).

[8] N.-K. Cho, J. Park, D. Lee, J.-W. Park, W.H. Lee, and Y.S. Kim, ACS Appl. Electron. Mater. **1**, 1698 (2019).

[9] Y.-H. Kim, J.-S. Heo, T.-H. Kim, S. Park, M.-H. Yoon, J. Kim, M.S. Oh, G.-R. Yi, Y.-Y. Noh, and S.K. Park, Nature **489**, 128 (2012).

[10] X. Yu, T.J. Marks, and A. Facchetti, Nat. Mater. **15**, 383 (2016).

[11] T. Sekitani, U. Zschieschang, H. Klauk, and T. Someya, Nat. Mater. **9**, 1015 (2010).

[12] J. Park, J.E. Huh, S.E. Lee, J. Lee, W.H. Lee, K.H. Lim, and Y.S. Kim, ACS Appl. Mater. Interfaces **10**, 30581 (2018).

[13] K.-H. Lim, K. Kim, S. Kim, S.Y. Park, H. Kim, and Y.S. Kim, Adv. Mater. **25**, 2994 (2013).

[14] E. Fortunato, P. Barquinha, and R. Martins, Adv. Mater. **24**, 2945 (2012).

[15] J.S. Park, W.J. Maeng, H.S. Kim, and J.S. Park, Thin Solid Films **520**, 1679 (2012).

[16] J. F. Wager, D. A. Keszler, and R. E. Presley, *Transparent Electronics* (Springer, New York, 2008)

[17] W. E. Spear, P. G. Lecomber, Solid State Commun. **88**, 1015 (1993)

[18] Y.J. Tak, F. Hilt, S. Keene, W.G. Kim, R.H. Dauskardt, A. Salleo, and H.J. Kim, ACS Appl. Mater. Interfaces **10**, 37223 (2018).

[19] B.S. Kim and H.J. Kim, IEEE Trans. Electron Devices **63**, 3558 (2016).

[20] M.G. Kim, M.G. Kanatzidis, A. Facchetti, and T.J. Marks, Nat. Mater. **10**, 382 (2011).

[21] T. Iwasaki, N. Itagaki, T. Den, H. Kumomi, K. Nomura, T. Kamiya, and H. Hosono, Appl. Phys. Lett. **90**, 1 (2007).

[22] K.K. Banger, Y. Yamashita, K. Mori, R.L. Peterson, T. Leedham, J. Rickard, and H. Sirringhaus, Nat. Mater. **10**, 45 (2011).

[23] R. Chen and L. Lan, Nanotechnology **30**, (2019) 312001.

[24] H. Hosono, J. Non. Cryst. Solids **352**, 851 (2006).

[25] T. Kamiya and H. Hosono, NPG Asia Mater. **2**, 15 (2010).

[26] K. Nomura, H. Ohta, K. Ueda, T. Kamiya, M. Hirano, and H. Hosono, Science (80-.). **300**, 1269 (2003).

[27] K. Nomura, H. Ohta, A. Takagi, T. Kamiya, M. Hirano, and H. Hosono, Nature **432**, 488 (2004).

[28] T.-M. Pan, B.-J. Peng, J.-L. Her, B.-S. Lou, IEEE Trans. Electron Devices **64**, 2233 (2017).

[29] M. Benwadih, J. Chroboczek, G. Ghibaudo, R. Coppard, D. Vuillaume, J. Appl. Phys. **115**, 214501 (2014).

[30] T. Kamiya, K. Nomura, M. Hirano, H. Hosono, Phys. Status Solidi C **5**, 3098 (2008).

[31] Y. Kim, M. Bae, W. Kim, D. Kong, H. K. Jung, H. Kim, S. Kim, D. M. Kim, D. H. Kim, IEEE Trans. Electron Devices **59**, 2689 (2012).

[32] T. Kamiya, K. Nomura, H. Hosono, Phys. Status Solidi A **206**, 860 (2009).

[33] M. Li, J. Zheng, H. Xu, Z. Wang, Q. Wu, B. Huang, H. Zhou, and C. Liu, Adv. Mater. Interfaces **5**, 1 (2018).

[34] T. Kamiya, K. Nomura, and H. Hosono, J. Disp. Technol. **5**, 273 (2009).

[35] R.M. Pasquarelli, D.S. Ginley, and R. O'Hayre, Chem. Soc. Rev. **40**, 5406 (2011).

[36] Y.S. Rim, H. Chen, T. Bin Song, S.H. Bae, and Y. Yang, Chem. Mater. 27, 5808 (2015).

[37] S. Jeong, J.Y. Lee, S.S. Lee, S.W. Oh, H.H. Lee, Y.H. Seo, B.H. Ryu, and Y. Choi, J. Mater. Chem. **21**, 17066 (2011).

[38] E.G. Lee, J. Park, S.-E. Lee, J. Lee, C. Im, G. Yoo, J. Yoo, and Y.S. Kim, Appl. Phys. Lett. **114**, 172903 (2019).

[39] H.J. Na, N.K. Cho, J. Park, S.E. Lee, E.G. Lee, C. Im, and Y.S. Kim, J. Mater. Chem. C **7**, 14223 (2019).

[40] S.-E. Lee, J. Park, J. Lee, E.G. Lee, C. Im, H. Na, N.-K. Cho, K.-H. Lim, and Y.S. Kim, ACS Appl. Electron. Mater. **1**, 430 (2019).

[41] B.N. Pal, B.M. Dhar, K.C. See, and H.E. Katz, Nat. Mater. **8**, 898 (2009).

[42] J. Robertson, Reports Prog. Phys. **69**, 327 (2006).

[43] W.J. Park, H.S. Shin, B. Du Ahn, G.H. Kim, S.M. Lee, K.H. Kim, and H.J. Kim, Appl. Phys. Lett. **93**, 2006 (2008).

[44] J.E. Huh, J. Park, J. Lee, S.E. Lee, J. Lee, K.H. Lim, and Y.S. Kim, J. Ind. Eng. Chem. **68**, 117 (2018).

[45] J. Kolodzey, Guohua Qui, I. Rau, E.A. Chowdhury, J.O. Olowolafe, T.N. Adam, J.S. Suehle, and Yuan Chen, IEEE Trans. Electron Devices **47**, 121 (2002).

[46] J. Lee, J. Lee, J. Park, S.-E. Lee, E.G. Lee, C. Im, K.-H. Lim, and Y.S. Kim, ACS Appl. Mater. Interfaces **11**, acsami.8b18422 (2019).

Chapter 2

High Performance Solution-Processed Oxide Thin-Film Transistors through Atmospheric-Pressure Plasma Treatment

2.1 Introduction

Oxide semiconductors (OSs) have attracted great interest as a channel layer of thin-film transistor (TFT) in future display due to their good electrical and unique properties such as high optical transparency and flexibility. [1-3] In particular, low-temperature solution-processed OSs have been widely investigated because they can be fabricated quickly and cheaply on a flexible substrate by advanced processes including ink-jet printing and the roll-to-roll process. [4,5] Recently, high-performance solution-processed OS TFTs with high field-effect mobility can be realized through various novel methods such as sol-gel on chip, combustion, and ultraviolet (UV) radiation. [6-8]

In particular, the aqueous route method has realized solution-processed indium oxide (InO_x) TFTs with a remarkably high field-effect mobility (> 10 cm^2/Vs) despite being fabricated with a low temperature (< 300 °C) process, which has shown new possibilities for practical application of solution-processed OS TFTs. [9,10] However, despite the excellent electrical properties with high field-effect mobility, the application of a solution-processed OS TFTs still remains a difficult task as a practical technology due to the major disadvantages of current ratio. In conventional display technology, the V_{on} and on/off current ratio are as important as the field-effect mobility of the TFT because they are strongly related to power consumption of the device in practical

industrial application. The V_{on} and on/off current ratio of TFT are determined in consideration of various factors such as thickness, trap density, gate metal type and carrier concentration of a semiconductor. Among them, in practical TFT applications, the V_{on} and the on/off current ratio are mainly controlled by the carrier concentration of a semiconductor. For this reason, the control of carrier concentration of semiconductor is essential for the practical application of solution-processed OS TFTs.

In vacuum-processed OS TFTs such as indium gallium zinc oxide (IGZO) TFT used in display technology, gallium atom in IGZO has been used to control the carrier concentration of OSs because it has a stronger bonding with oxygen than indium or zinc. [11,12] In general, the addition of gallium atoms to OSs lowers the mobility of the TFTs. Since the vacuum-processed OS TFT has a sufficiently high field-effect mobility to compensate for the decrease in mobility, the decrease is not so fatal when applying vacuum-processed OS TFTs to display technology. However, the addition of gallium in the solution-processed OS TFT cannot be a simple solution. Although solution-processed OS TFTs with a high field-effect mobility have recently been developed with various methods, they still show much lower field-effect mobility in comparison to vacuum process OS TFTs because they have many defects due to the limitations of a solution process. Accordingly, the decrease in field-effect mobility by the addition of gallium can be fatal because the solution-processed OS TFTs fail to achieve

enough high mobility that is required for application in practical display technology. [13,14] As another method, conventional plasma treatment in vacuum conditions has been studied for controlling the carrier concentration of OSs, since oxygen plasma treatment controls the oxygen vacancy associated with the carrier concentration in OS. Several studies have demonstrated that conventional vacuum plasma treatment improves the electrical properties of TFTs with V_{on} and on/off current ratio depending on the carrier concentration. [15-17] Unfortunately, conventional oxygen plasma treatment essentially requires the vacuum conditions to activate the plasma state, which makes it difficult to apply the conventional plasma treatment to solution-process OSs because the introduction of a vacuum process strongly loses the advantages of the solution process, such as the formation in ambient conditions. Accordingly, there is a growing demand for a technique capable of adjusting the carrier concentration suitable for application to high-performance solution-processed OSs in a practical industry.

Herein, I propose an effective atmospheric-pressure plasma (APP) treatment for simple and effective control of the carrier concentrations and important TFT parameters of solution-processed OS TFTs, such as V_{on} and on/off current ratio. I have successfully implemented the improvements in important TFT parameters, V_{on} from -11.4 V to -1.9 V and the on/off current ratio from ~10^3 to ~10^6, which still keep up the high field-effect mobility (> 20 cm^2/Vs), by

introducing the APP treatment into solution-processed InO_x TFTs fabricated at low temperature condition (~ 250 °C). Based on various analyses such as X-ray photoelectron spectroscopy (XPS), electrical characterization, and UV-Visible spectroscopy, I identified that the APP treatment can effectively control oxygen vacancy and carrier concentration in solution-processed OS. To the best of our knowledge, this is the first introduction of the APP treatment to faithfully control the electrical properties of the solution-processed OS TFTs while maintaining the advantages of the solution process. These results show that the APP treatment has a great potential for significantly modulating the electrical properties of solution-processed OS TFTs.

2.2 Fabrication of oxide semiconductor thin-film transistors

Figure 2.1 shows the schematic of the solution-process OS TFTs fabrication process. InO_x films were prepared by a spin coating process with precursor solutions (0.1, 0.15, 0.2, 0.25, and 0.3 M) and an annealing process of 250 °C with a tube furnace. They showed various thicknesses of 4.9, 6.5, 8.7, 10.6, and 12.9 nm, respectively (Figure 2.2). Then, the prepared InO_x thin films are post-treated by the APP treatment. For an effective APP treatment, several key variables including film thickness, substrate temperature, plasma source power and treatment time must be carefully considered. Considering the changes in the electrical characteristics of the InO_x TFTs, due to the thinner thickness of the InO_x films, the greater change in electrical properties of the InO_x TFT was induced by the APP process (Figure 2.3). However, at 10 nm or less, the effected changes were not significantly different. Accordingly, in this study, a thickness of less than 10 nm thin film coated with 0.15 M InO_x precursor solution was mainly focused because it exhibits the highest mobility while suppressing the decrease of mobility by the APP treatment. Also, in view of the several key variables of the electrical characteristics of the InO_x TFTs depending on the APP treatment, experimental conditions including the substrate temperature (150, 200, and 250 °C), plasma source power (500, 600, and 700 W), and APP treatment time (1, 3, 5, and 7 min) were changed. All of these variables affected

the electrical properties of the InO_x TFTs, but the effect of APP treatment time was the most obvious (Figures 2.4, 2.5). Thus, to effectively analyze the effect of APP treatment, the APP treatment time was controlled as a main variable under optimized conditions with substrate temperature (200 °C) and APP source power (700 W).

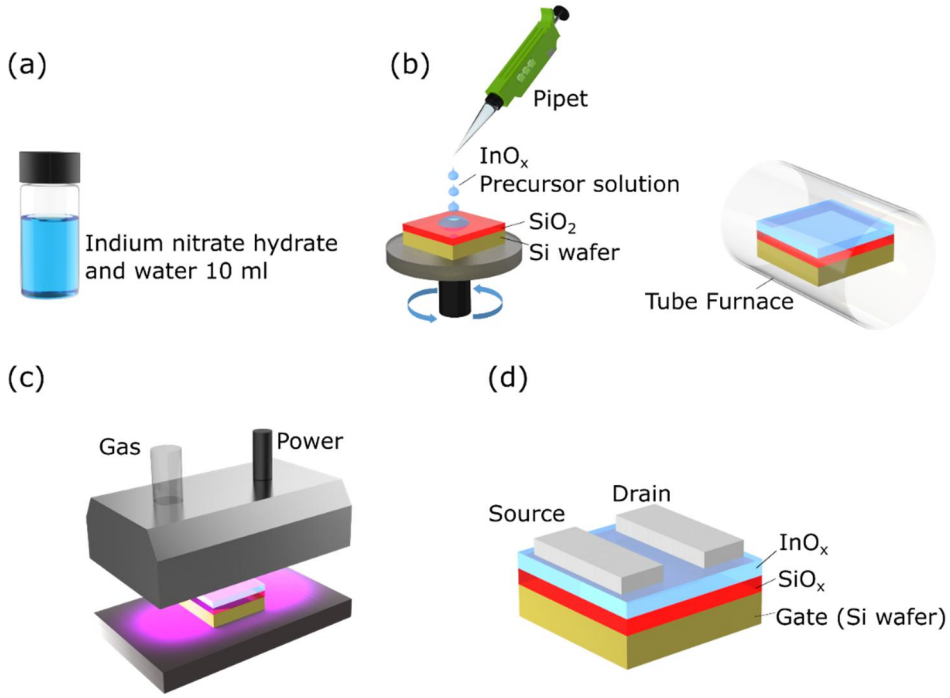

Figure 2. 1 Simplified schematics of our experimental procedures. a) Prepared InO_x precursor solution. b) Spin-coating of InO_x onto Si/SiO_2 substrate followed by thermal annealing at 250 °C. c) Plasma treatment in air. d) Thermally evaporated Al source-drain electrodes through shadow masks.

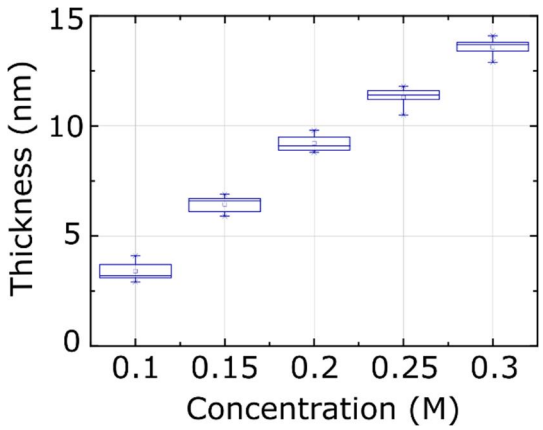

Figure 2. 2 Thickness analyses by varying the molar concentration of the precursor solution using reflectometer (ST2000-DLXn, K-MAC Co.).

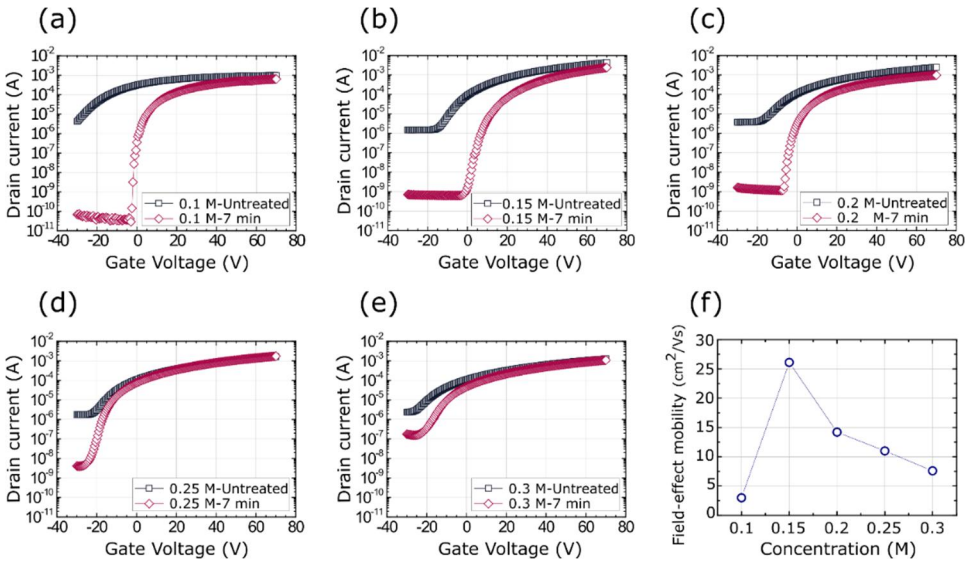

Figure 2. 3 The transfer characteristics of untreated InO_x and 7 min atmospheric-pressure plasma treated TFTs fabricated at various molar concentration precursors of (a) 0.1 M, (b) 0.15 M, (c) 0.2 M, (d) 0.25 M, and (e) 0.3 M. (f) The variation of the field-effect mobility in InO_x TFTs according to the concentration of the In-based aqueous solution

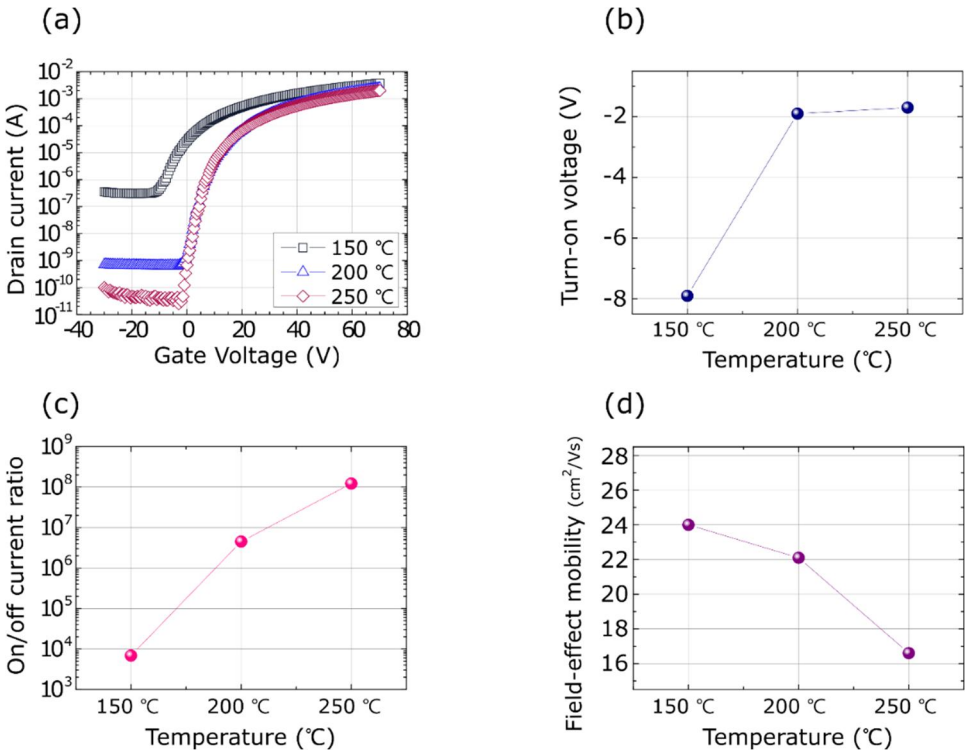

Figure 2. 4 The transfer characteristics of InO_x TFTs varying the substrate temperature. (a) Transfer characteristics, (b) turn-on voltage, (c) on/off current ratio, (d) field-effect mobility. The atmospheric-pressure plasma treatment time is fixed at 7 min.

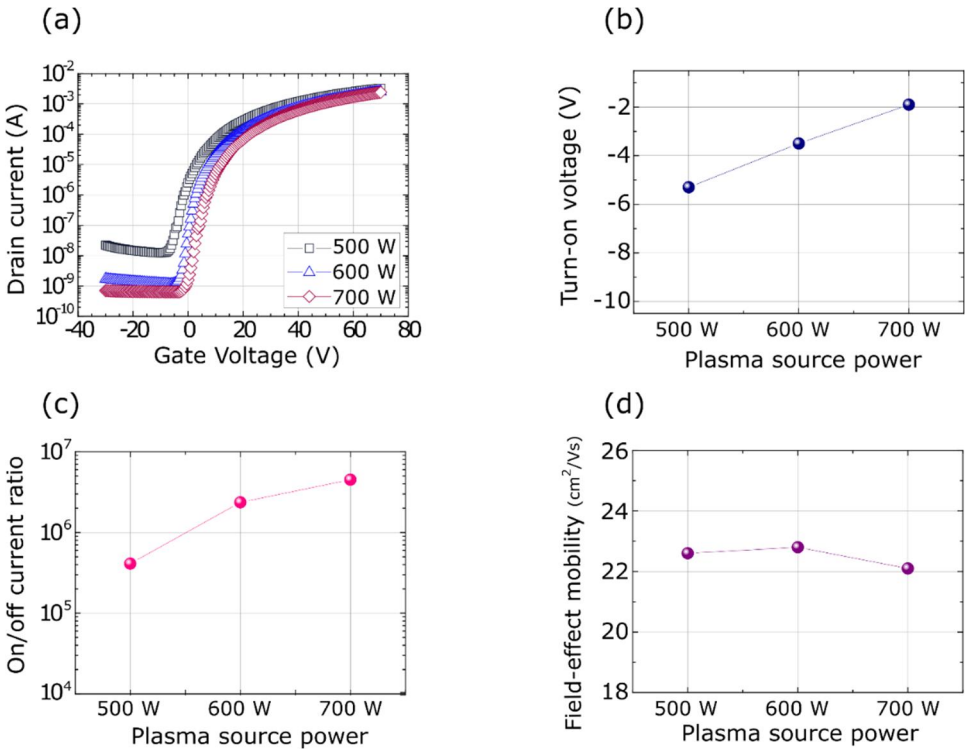

Figure 2. 5 The transfer characteristics of InO_x TFTs varying the plasma source power. (a) Transfer characteristics, (b) turn-on voltage, (c) on/off current ratio, (d) field-effect mobility. The atmospheric-pressure plasma treatment time is fixed at 7 min.

2.3 Analysis of chemical properties of plasma treated film

Figure 2.6 and Figure 2.7 show the chemical changes in the InO_x film depending on the APP treatment. The XPS analyses show a consistent tendency for a change in the O 1s spectrum of InO_x films depending on the APP treatment time. For further analysis, the O 1s spectrum was fitted by the Gaussian-Lorentzian function. The O 1s spectrum of InO_x thin films could be divided into three peaks centered at 532, 531.15, and 529.8 eV which were assigned to the oxygen bond of the hydroxide (O-H bond), the oxygen vacancy (O_{vac}), and metal oxide without oxygen vacancy (M-O bond), respectively. [8,18] The Ovac/(Ovac + M-O bond) area ratios for APP-untreated and APP-treated InO_x thin films are 0.342 (untreated), 0.305 (3 min), and 0.267 (7 min) (Table 3.1). It can be confirmed that the oxygen vacancy of InO_x is reduced by the increase of APP treatment time, which means that APP effectively affects the chemical properties of solution-processed InO_x thin films. Typically, in the OSs, oxygen vacancy acts as a shallow donor, one of the main factors controlling the carrier concentration of OSs and the electrical properties of OS TFTs.

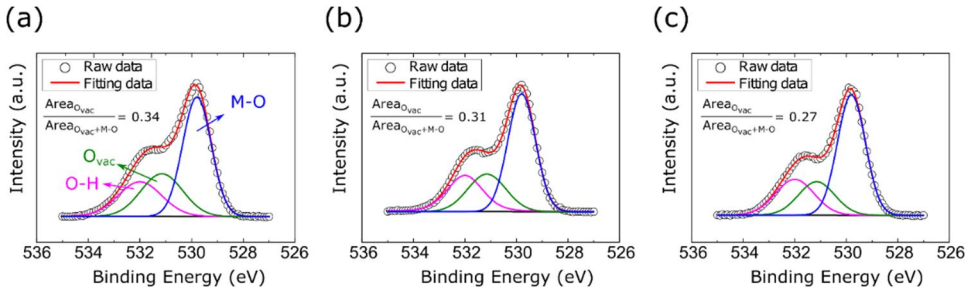

Figure 2. 6 The O 1s XPS spectra for a) the untreated, b) the 3 min APP treated, and c) the 7 min APP treated InO_x thin film.

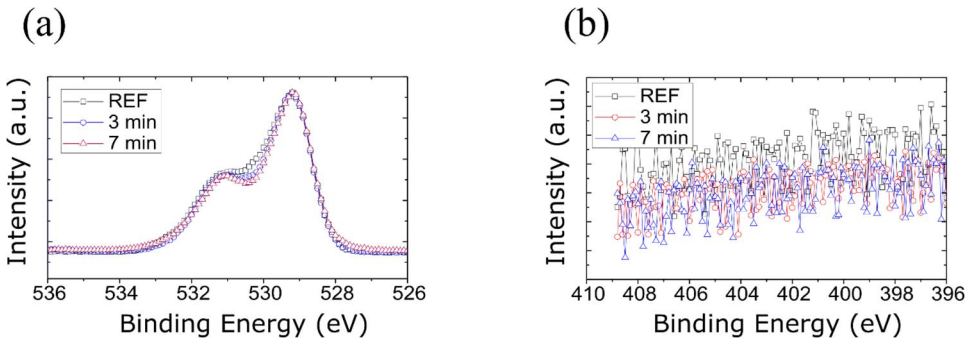

Figure 2. 7 The XPS spectra of O 1s (a) and N 1s (b) for the untreated, the 3 min atmospheric-pressure plasma treated, and the 7 min atmospheric-pressure plasma treated InO_x thin film. The nitrogen component was not detected in all the samples.

	REF	3 min	7 min
$Area_{O\text{-}VAC}$ / $Area_{(O\text{-}VAC + M\text{-}O)}$	0.34	0.31	0.27
$Area_{O\text{-}VAC}$ / $Area_{M\text{-}O}$	0.52	0.44	0.37

Table 2. 1 The ratio of O_{vac} bond area to (O_{vac} + M-O) bond area and O_{vac} bond area to M-O bond area by varying plasma treatment time.

2.4 Electrical characterization of InO_x TFTs

Actually, in InO_x TFT transfer characteristics in the linear region with the gate-source voltage (V_{gs}) sweep from -30 to 70 V and drain voltage (V_d) of 10 V, it can be confirmed that physical parameters of the InO_x TFT including V_{on} and on/off current ratio were prominently changed according to the changes in APP treatment time (Figure 2.8). As APP treatment time is increased, the V_{on} and on/off current ratio was significantly changed. The APP-treated TFTs are shown as V_{on} of -10.7 V for 1 min, -5.8 V for 3 min, -4.8 V for 5 min, and -1.9 V for 7 min. Here, V_{on} means V_{gs} value where drain current (I_d) starts to increase. Also, the APP-treated TFTs are shown as an on/off current ratio of ~10^4 for 1 min, ~10^4 for 3 min, ~10^5 for 5 min, and ~10^6 for 7 min. Compared with the untreated InO_x TFTs with V_{on} of -11.4 V and on/off current ratio of ~10^3, the APP-treated InO_x TFTs show the strongly improved V_{on} and on/off current ratio values. Meanwhile, although the magnitude of the change is not large, field-effect mobility of InO_x TFTs is slightly decreased by the APP treatment. The field-effect mobility of InO_x TFTs with 26.1 $cm^2 V^{-1} s^{-1}$ decreased to 24.3 $cm^2 V^{-1} s^{-1}$ for 1 min, 23.7 $cm^2 V^{-1} s^{-1}$ for 3 min, 23.6 $cm^2 V^{-1} s^{-1}$ for 5 min, and 22.1 $cm^2 V^{-1} s^{-1}$ for 7 min.

Importantly, the decrease in field-effect mobility of the InO_x TFT by the APP method is considered to be relatively small in comparison with the decreasing

behavior of the field effect mobility of the InO_x TFT according to the doping method for improving the on/off current ratio and V_{on} of the OS TFT. I speculate that the APP treatment has more effect on oxygen vacancies forming deep traps which is far from the conduction band minimum (CBM) than oxygen vacancies acting as a shallow donor state close to CBM, which strongly affects the change of field effect mobility. [19] The changes of electrical properties coincide with the tendency to be induced by the change of oxygen vacancy contents, which implies that the reduction oxygen vacancy by the APP treatment effectively decrease the carrier concentration of the InO_x thin film. A summary of statistical values of electrical characteristics obtained from the current-to-voltage characteristics are listed in Table 3.2.

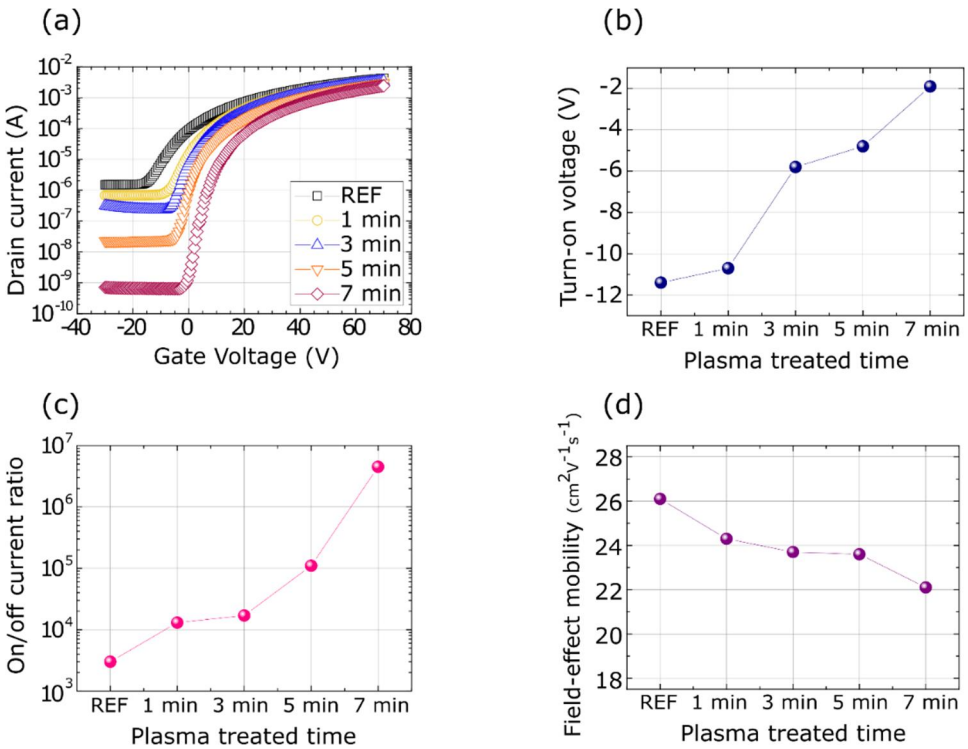

Figure 2. 8 The transfer characteristics and the change in TFT parameters of InO_x TFTs depending on APP treatment time. a) Transfer characteristics, b) turn-on voltage, c) on/off current ratio, d) field-effect mobility.

	REF	1 min	3 min	5 min	7 min
Field-effect mobility (cm^2/Vs) <σ>	26.1 <0.55>	24.3 <0.25>	23.7 <0.31>	23.6 <0.14>	22.1 <0.14>
On/off current ratio	$3.0x10^3$	$1.3x10^4$	$1.7x10^4$	$1.1x10^5$	$4.5x10^6$
Turn-on voltage (V) <σ>	-11.4 <2.05>	-10.7 <1.69>	-5.8 <1.20>	-4.8 <0.51>	-1.9 <0.49>

Table 2. 2 Field-effect mobility, on/off current ratio, and turn-on voltage of InO_x TFTs with atmospheric plasma treatment in 25 samples by one-run.

2.5 Activation energy and optical band gap of InO_x

To verify the change in carrier concentration of InO_x thin film according to the APP treatment, the behavior in activation energy and optical band gap of InO_x according to the APP treatment was investigated. To extract the activation energy, the transfer characteristics of the InO_x TFTs were obtained at 133, 173, 213, 253 and 298 K under a vacuum environment (Figure 2.9). Activation energy (E_a) can be obtained by field-effect mobility and $\ln(\mu_{FET})$-1000/T plot depending on V_{gs} and temperature, as shown in Figure 2.10a-b. At the same V_{gs} condition (10 V), it is confirmed that the activation energy of InO_x increases in accordance with the APP treatment processing time, which means that the Fermi level of InO_x TFT is shifted by the APP treatment. It can be seen that the longer the plasma treatment time, the lower the Fermi level of InO_x. Typically, in the n-type OS based TFT, when the V_{gs} increases, the localized states are filled with accumulated carriers and the Fermi level is closed with the mobility edge, which results in the decrease of the activation energy. [20,21] Actually, at higher V_{gs} conditions, APP-treated InO_x has similar activation energy in comparison to untreated InO_x. Through the plasma treatment, it can be confirmed that the activation value of InO_x at each V_{gs} moves almost perfectly parallel to the V_{gs} direction. The results show that the carrier concentration of InO_x is decreased by the APP treatment without changing the localized states near the Fermi level.

Generally, as the trend of optical band gap in InO_x depending on the APP treatment is similar to that of the activation energy for OS TFTs, I analyze the change of optical band gap in InO_x depending on the APP treatment. The transmittance spectra of the InO_x thin films on quartz substrate are shown in Figure 2.10c. As compared to untreated InO_x, slight red shifts in the transmittance of APP treated InO_x were observed. To investigate the phenomenon in more detail, the optical band gap is extracted by the Tauc relation [22,23] as follows:

$$(\alpha hv)^m = A(hv - E_g)$$

where *hv* is the photon energy and A is a constant. Although the m value of 1/2 is commonly used for non-direct semiconductor, in this study, I applied the m value of 2, which is used in direct semiconductor model, to examine the small changes of optical band gap in more detail. The variation of the $(\alpha h\nu)^2$ versus the photon energy in the absorption region is plotted for the samples in Figure 2.10d, and extrapolation of linear fit to the photon energy axis at $(\alpha h\nu)^2 = 0$ gives the optical band gap. As a result, it can be seen that the longer the plasma treatment time, the smaller the optical band gap of InO_x. According to the Burstein-Moss effect, because the doubly occupied state is limited by the Pauli principle and the optical transition should be vertical, extra energy is required to enable the valence electrons to move to higher energy states in the conduction band, which causes the increase of optical band gap according to the increase of

carrier concentration. [24-27] In this respect, it is deduced that the decrease in the optical band gap of InO_x is induced by the decrease in the carrier concentration in InO_x with the APP treatment, which agrees with the tendency of electrical characteristic change in InO_x TFTs according to the APP treatment. Overall, analyses with the behavior in activation energy and optical band gap of InO_x according to the APP treatment imply that the carrier concentration of InO_x is decreased by the APP treatment, which is consistent with the tendency of oxygen vacancies of InO_x to change with the APP treatment, and is confirmed by XPS analysis. This shows that possibility the APP treatment can control the carrier concentration of the OSs as the APP treatment controls the oxygen vacancy of the OSs

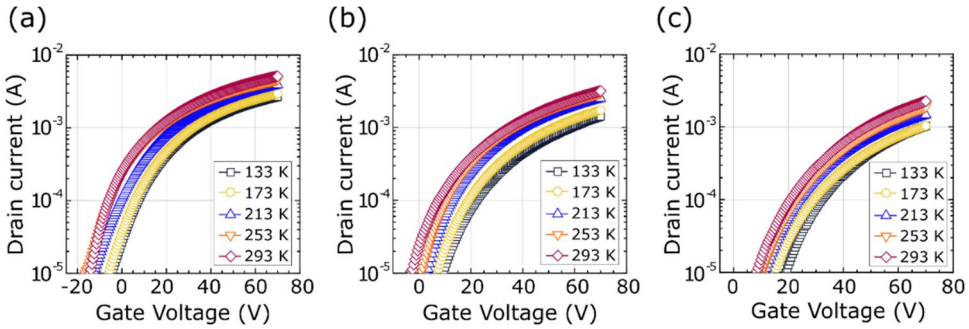

Figure 2. 9 At 133 K, 173 K, 213 K, 253 K, and 293 K, the transfer characteristics of (a) untreated sample, (b) 3 min plasma treated sample, and (c) 7 min plasma treated sample.

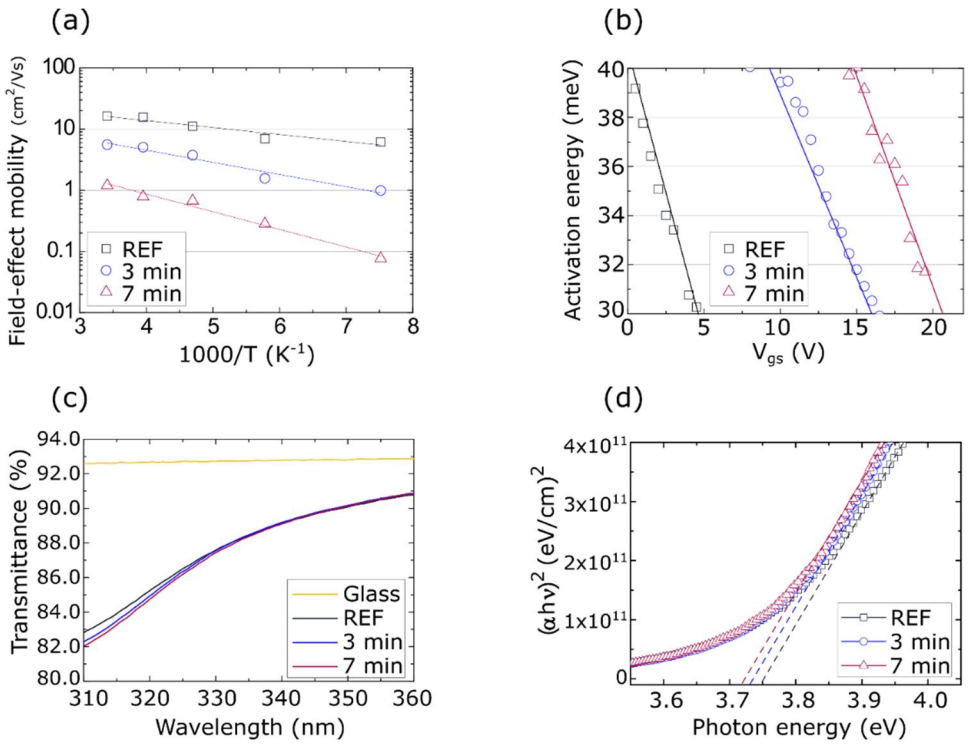

Figure 2. 10 a) An example of $\ln(\mu_{eff})$ – (1000/T) plot with linear fit at applied V_{gs} of 10 V, b) the activation energy as a function of the APP treatment time. c) The optical transmittance of glass and InO_x films as a function of the APP treatment time, d) the $(\alpha h\nu)^2$ versus the photon energy plot of the InO_x films.

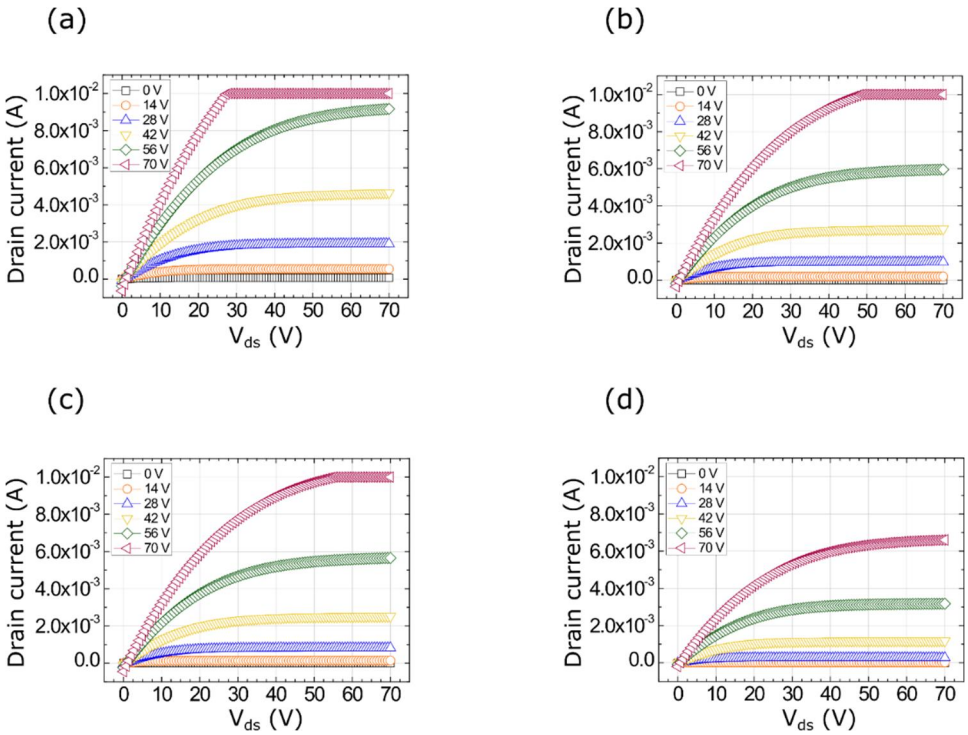

Figure 2. 11 The output characteristics of (a) untreated sample, (b) 3 min APP-treated sample, (c) 5 min APP-treated sample, and (d) 7 min APP-treated sample. Our current compliance of analyzer (Agilent 4155B) is 0.01 A.

2.6 Conclusion

Generally, in the display industry, conventional APP is mainly used for surface treatment. In fact, it has been reported that the electrical properties of IGZO fabricated by a vacuum process are not greatly changed when treated with conventional APP. Otherwise, our results show that APP can significantly control the electrical properties of solution-processed OS TFTs. I may conclude that the APP has a significant effect on the solution-processed OSs because the density of solution-processed semiconductors is relatively low. Actually, the low density and thin thickness, ~ 10 nm, of solution-processed OS shows other advantages in application to flexible substrates. [21,28] In this part, in-depth research is ongoing.

In summary, I newly introduce the potential of an APP treatment that can simply and effectively control the carrier concentration of solution-processed OS thin film. With an effective APP treatment, I demonstrate that important electrical properties for power consumption, such as V_{on} and the on/off current ratio, of solution-processed InO_x TFT fabricated at low temperature (~ 250 °C) can be controlled in atmosphere conditions while maintaining the high field-effect mobility (> 20 cm^2/Vs). Furthermore, because the V_{on} converges to 0 V and at the same time the on/off current ratio is maximized (~10^6), this APP technique can provide significant advances toward industrial applications of

solution-processed OS TFTs, while maintaining the advantages of the solution process.

2.7 Experimental details

Synthesis and Characterization of Precursor OS Solution: InO_x precursor solutions (0.1, 0.15, 0.2, 0.25, and 0.3 M) were prepared by dissolving indium nitrate hydrate in 10 mL of 18.2 MΩ deionized water, and then the solution was stirred at 500 rpm for 3 days at 25 °C. The precursor solution was filtered through a 0.22 mm syringe filter PTFE, and was spin coated onto a heavily doped P-type Si wafer with 200 nm thick SiO_2 gate dielectric layer at a speed of 5000 rpm for 30 s under a humidity of 10 %. Then the films were soft-baked at 250 °C for 60 s, and were annealed in a tube furnace under <10% humidity at 250 °C for 8 hours. Afterwards, the films were plasma-treated with atmospheric-pressure plasma equipment in the range between 0 and 7 minutes in the atmosphere (Multi-Layer Electrode, PSM Inc. Figure 2.12). The distance between plasma source and sample was 5 mm. Nitrogen and CDA (compressed dry air) were used for the plasma generation and flow rates were 200 ℓ/min and 0.7 ℓ/min, respectively. X-ray photoelectron spectroscopy (XPS) (SIGMA PROBE, ThermoVG) was used to obtain the electronic state of the InO_x films. UV-Visible spectrometer (Lambda 35, PerkinElmer) was used to characterize the optical properties.

Fabrication and Characterization of OS TFTs: The aluminum source and drain electrodes were deposited on the InO_x layer by thermal evaporation with a thickness of 100 nm, width of 1000 μm, and length of 50 μm through shadow

masks. The transfer characteristics of InO_x TFT were measured by a semiconductor parameter analyzer (Agilent 4155B) under dark and ambient condition. The field-effect mobility of the TFTs was evaluated by a linear formula.

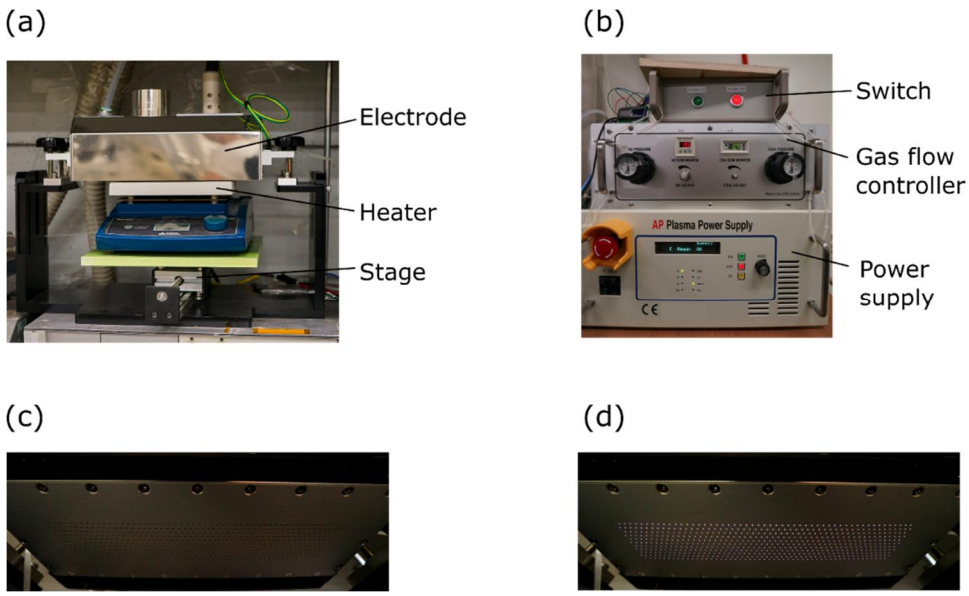

Figure 2. 12 Actual photo of atmospheric-pressure plasma system used in this experiment. (a) Plasma electrode and heating stage. (b) Gas flow control unit and power supply. (c), (d) Plasma electrode before and after activating plasma.

2.8 References

[1] E. Fortunato, P. Barquinha, and R. Martins, Adv. Mater. **24**, 2945 (2012).

[2] S.Y. Park, B.J. Kim, K. Kim, M.S. Kang, K.H. Lim, T. Il Lee, J.M. Myoung, H.K. Baik, J.H. Cho, and Y.S. Kim, Adv. Mater. **24**, 834 (2012).

[3] P.K. Nayak, Z. Wang, and H.N. Alshareef, Adv. Mater. **28**, 7736 (2016).

[4] D.H. Lee, Y.J. Chang, G.S. Herman, and C.H. Chang, Adv. Mater. **19**, 843 (2007).

[5] Y.S. Rim, H. Chen, X. Kou, H.S. Duan, H. Zhou, M. Cai, H.J. Kim, and Y. Yang, Adv. Mater. **26**, 4273 (2014).

[6] K.K. Banger, Y. Yamashita, K. Mori, R.L. Peterson, T. Leedham, J. Rickard, and H. Sirringhaus, Nat. Mater. **10**, 45 (2011).

[7] M.G. Kim, M.G. Kanatzidis, A. Facchetti, and T.J. Marks, Nat. Mater. **10**, 382 (2011).

[8] Y.-H. Kim, J.-S. Heo, T.-H. Kim, S. Park, M.-H. Yoon, J. Kim, M.S. Oh, G.-R. Yi, Y.-Y. Noh, and S.K. Park, Nature **489**, 128 (2012).

[9] Y. Hwan Hwang, J.-S. Seo, J. Moon Yun, H. Park, S. Yang, S.-H. Ko Park, and B.-S. Bae, NPG Asia Mater. **5**, e45 (2013).

[10] K.H. Lim, J.E. Huh, J. Lee, N.K. Cho, J.W. Park, B. Il Nam, E. Lee, and Y.S. Kim, ACS Appl. Mater. Interfaces **9**, 548 (2017).

[11] T. Iwasaki, N. Itagaki, T. Den, H. Kumomi, K. Nomura, T. Kamiya, and H. Hosono, Appl. Phys. Lett. **90**, 1 (2007).

[12] T. Kamiya and H. Hosono, NPG Asia Mater. **2**, 15 (2010).

[13] X. Yu, T.J. Marks, and A. Facchetti, Nat. Mater. **15**, 383 (2016).

[14] S. Jeong, Y.G. Ha, J. Moon, A. Facchetti, and T.J. Marks, Adv. Mater. **22**, 1346 (2010).

[15] J.S. Kim, M.K. Joo, M. Xing Piao, S.E. Ahn, Y.H. Choi, H.K. Jang, and G.T. Kim, J. Appl. Phys. **115**, (2014).

[16] H. Pu, Q. Zhou, L. Yue, and Q. Zhang, Appl. Surf. Sci. **283**, 722 (2013).

[17] J.S. Park, J.K. Jeong, Y.G. Mo, H.D. Kim, and S. Il Kim, Appl. Phys. Lett. **90**, 1 (2007).

[18] P.K. Nayak, M.N. Hedhili, D. Cha, and H.N. Alshareef, Appl. Phys. Lett. **103**, 033518 (2013).

[19] M. Li, J. Zheng, H. Xu, Z. Wang, Q. Wu, B. Huang, H. Zhou, and C. Liu, Adv. Mater. Interfaces **5**, 1 (2018).

[20] C.G. Lee, B. Cobb, and A. Dodabalapur, Appl. Phys. Lett. **97**, 2008 (2010).

[21] K.-H. Lim, J. Lee, J.-E. Huh, J. Park, J.-H. Lee, S.-E. Lee, and Y.S. Kim, J. Mater. Chem. C **5**, 7768 (2017).

[22] S.W. Xue, X.T. Zu, W.L. Zhou, H.X. Deng, X. Xiang, L. Zhang, and H. Deng, J. Alloys Compd. **448**, 21 (2008).

[23] J. Lü, J. Dai, J. Zhu, X. Song, and Z. Sun, J. Wuhan Univ. Technol. Sci. Ed. **26**, 23 (2011).

[24] B.E. Sernelius, K.F. Berggren, Z.C. Jin, I. Hamberg, and C.G. Granqvist, Phys. Rev. B **37**, 10244 (1988).

[25] J. Socratous, K.K. Banger, Y. Vaynzof, A. Sadhanala, A.D. Brown, A. Sepe, U. Steiner, and H. Sirringhaus, Adv. Funct. Mater. **25**, 1873 (2015).

[26] C.E. Kim, P. Moon, S. Kim, J.M. Myoung, H.W. Jang, J. Bang, and I. Yun, Thin Solid Films **518**, 6304 (2010).

[27] K.-H. Lim, K. Kim, S. Kim, S.Y. Park, H. Kim, and Y.S. Kim, Adv. Mater. **25**, 2994 (2013).

[28] T. Sekitani, U. Zschieschang, H. Klauk, and T. Someya, Nat. Mater. **9**, 1015 (2010).

Chapter 3

High Quality Solution-Processed Gate Dielectric Films in Thin-Film Transistors through Atmospheric-Pressure Plasma Treatment

3.1 Introduction

Thin-film transistors (TFTs) used as switching devices in the display industry are generally fabricated by depositing electrodes, dielectrics, and semiconductor materials onto substrates such as Si wafer, glass, or flexible films. [1-3] These thin films are successfully deposited in a vacuum atmosphere using various methods including radio frequency magnetron sputtering, atomic layer deposition and pulsed laser deposition. Nevertheless, the vacuum equipment is cumbersome, expensive, and difficult to fabricate in large scale, simple and cheap solution process techniques such as combustion, spray pyrolysis, ink-jet, and spin coating and have been mounting interest as thin film deposition methods. Among them, an aqueous route method capable of depositing a high-quality thin film at a relatively low temperature (~ 300 °C) by a simple process has been actively studied. [4,5] However, studies on thin films using the aqueous route method are mostly concentrated on oxide semiconductors. Research on dielectrics is also mainly based on a vacuum process, which causes problems in process unity with a semiconductor thin film deposited by a solution process. [6] Accordingly, research on improving the characteristics of solution-processed dielectrics, which is an essential component of the TFT structure, is urgently required.

In general, high-k materials such as AlO_x, YO_x, TaO_x, HfO_x, and ZrO_x have

been investigated as dielectric layers in TFTs because they can provide large gate capacitance without significantly increasing gate leakage current. [7,8] In the midst of diverse dielectric materials, AlO_x has drawn considerable attention because of its low deposition temperature, low cost, transparency, and good compatibility with oxide semiconductors. [8,9] For these reasons, some researchers have been conducting studies to optimize the characteristics of solution-processed AlO_x dielectric films. Unfortunately, most studies have focused on optimizing parameters in the process or investigating precursors and solvents related to the formation of metal ligand complex, and the annealing temperature has risen to obtain high quality thin films. [10-13] Therefore, additional research is needed on how to obtain a high quality dielectric thin film at low temperature while maintaining the advantages of a solution process that does not use vacuum equipment. In previous work, I successfully controlled the electrical characteristics of the solution-processed oxide semiconductor through an atmospheric-pressure plasma treatment. [3,14] It was found that the chemical structure of the solution-processed thin film was considerably changed, which was affected by the atmospheric-pressure plasma (APP) treatment.

Herein, I propose an APP post-treatment technique that can effectively improve the electrical properties of the AlO_x dielectric film deposited by a solution process using the aqueous route method. Characteristic changes through the APP treatment were observed by a measurement of capacitance-

frequency and leakage current. The frequency dependency of AlO_x capacitance was reduced by the APP treatment. Also, as the APP treatment time increased, the leakage current density decreased. The root-mean-square surface roughness of all samples investigated by atomic force microscopy (AFM) is in the range of 0.12 to 0.16 nm and maintains an ultra-smooth surface regardless of the APP treatment. The changes of binding a relationship according to the APP treatment time were analyzed by X-ray photoelectron spectroscopy (XPS). Through the APP treatment, the aluminum oxide ratio of the AlO_x dielectric films was increased while the aluminum hydroxide ratio was decreased. Finally, TFTs including solution-processed AlO_x dielectric films were fabricated by depositing a solution-processed InO_x as a semiconductor film, and the characteristics were evaluated. The field-effect mobility of TFTs was increased from 9.77 $cm^2 V^{-1} s^{-1}$ to 26.79 $cm^2 V^{-1} s^{-1}$ due to the effect of the APP treatment on solution-processed AlO_x dielectric thin films. Moreover, for the APP-treated samples, the mobility remained constant over a wide frequency operating range. These results are valuable as a way to effectively improve the electrical characteristics of the dielectric thin film, which is an essential component of the TFTs, with a low temperature process condition while maintaining the advantages of the solution process.

3.2 Surface roughness of the AlO_x thin films

Figure 3.1 shows the surface roughness image of an AlO_x dielectric film deposited on a Si wafer according to the APP treatment time. The surface roughness of the dielectric film forming the interface between the dielectric film and the semiconductor film is one of the important factors that influence the carrier scattering and determine the characteristics of the device. [14,15] The root-mean-square surface roughness of all samples ranged from 0.12 to 0.16 nm, showing a very smooth surface regardless of the APP treatment. This smooth surface of the AlO_x film can help to form a good interface with the semiconductor film to be formed later. Actually, since the variation of the roughness with the increase of the APP treatment time is very small, it can be assumed that the change of the electrical characteristic at the interface due to the change of the surface roughness by the APP treatment is negligibly small.

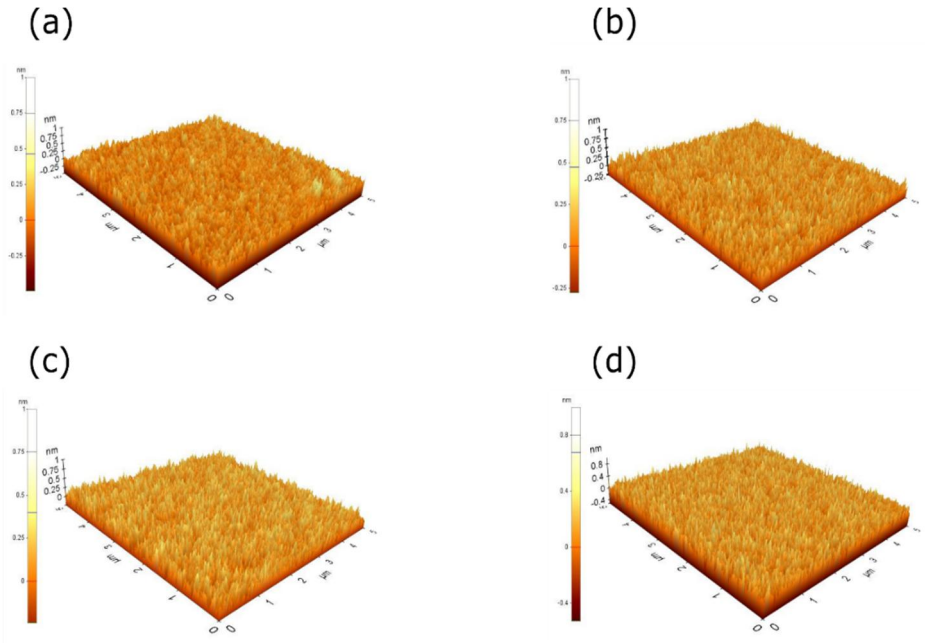

Figure 3. 1 AFM images for (a) the untreated, (b) the 7 minutes APP-treated, (c) the 9 minutes APP-treated, and (d) the 11 minutes APP-treated AlO_x thin film.

3.3 Analysis of electrical properties of the MIM devices

To investigate the dielectric properties of solution-processed AlO_x thin films, I first measured the frequency versus areal capacitance characteristics with varying the APP treatment time and annealing temperature using metal-insulator-metal (MIM) device (Figure 3.2). The untreated sample annealed at 250 ℃ (hereafter called REF) has an areal capacitance value between 451.8 nF cm^{-2} and 407.1 nF cm^{-2} when the frequency changes from 20 Hz to 100 kHz. The maximum capacitance value appears at 20 Hz, and the capacitance values tend to decrease gradually as the operating frequency increases. Typically, the dielectric film shows a constant capacitance value depending on the frequency. However, the capacitance value of the solution-processed dielectric film tends to vary strongly depending on the frequency. It is known that the mobile ions in AlO_x film easily form electrical double layers, so the capacitance value is influenced by the frequency. [6,16] On the other hand, the APP-treated AlO_x dielectric film is hardly dependent on frequency. Therefore, mobile ions in the AlO_x film are speculated to be removed effectively by the APP treatment. Moreover, the longer the APP treatment time is, the lower the capacitance value when compared to the REF. In particular, the capacitance value of the sample treated with the APP for 9 minutes after annealing at 250 ℃ had lower frequency dependence and was comparable to that of the sample annealed at 300 ℃. These

results provide clues to compatibility with flexible polymer substrates in the atmosphere by obtaining high-quality dielectric films at low temperature. The areal capacitance values of AlO_x thin film with various fabrication conditions are listed in Table 4.1.

The leakage current density of different AlO_x films is shown in Figure 3.3(a). The leakage current of the dielectric film in the TFTs has to be minimized for accurate switching operation and low power consumption. [17] Unfortunately, it is generally thought that the solution-processed dielectric film has a large leakage current density because the presence of large amounts of nitrate or hydroxyl groups leads to the conduction paths. [18-20] In this work, as shown in Figure 3.3(a), the leakage current density of AlO_x film was decreased obviously as the APP treatment time increased, which is attributed to the reduction of conduction paths. Particularly, with the same tendency as the capacitance-frequency measurement results, the leakage current density of the sample treated with the APP for 9 and 11 minutes after annealing at 250 ℃ was similar to that of the sample annealed at 300 ℃. The AlO_x films had a dielectric breakdown at electric fields between 2.5 and 3.5 MV/cm. (Figure 3.3 (b)) Also, the breakdown voltage of the AlO_x films became higher until the APP treatment time increased to 9 minutes and saturated hereafter. In comparison with the untreated sample (REF), the 9-minutes APP treated sample had a relatively low current density up to 3.3 MV/cm, which allowed a wide operating voltage of

devices, followed by drastically increasing current with dielectric breakdown field near 3.4 MV/cm. Interestingly, prior to breakdown, a change in the conduction mechanism of the leakage current is observed with plasma treatment time variation. According to Poole-Frankel emission and hopping-conduction model, the current densities are as follows, respectively [21,22]:

$$J_{PF} = q\mu N_c E \ \ exp\left[\frac{-q\left(\emptyset_T - \sqrt{qE/\pi\varepsilon_i\varepsilon_0}\right)}{kT}\right] \qquad (1)$$

$$J_h = qanv \ \ exp\left[\frac{qaE}{kT} - \frac{E_a}{kT}\right] \qquad (2)$$

where q is the electronic charge, μ is the electronic mobility, N_c is the density of states in the conduction band, $q\phi_T$ is the trap energy level, ε_i is the dielectric constant, ε_0 is the permittivity in vacuum, a is the mean hopping distance, k is the Boltzmann constant. Figure 3.3(c) and (d) show the plot of the current conduction mechanism with various AlO_x film treatment condition using equation (1) and (2). The untreated sample (REF) and 5-minute APP-treated samples follow Poole-Frankel emission mechanism whereas 9- and 11-minutes APP-treated samples are a good agreement with the hopping-conduction mechanism like the 300 °C annealed sample. Fitting using various dielectric conduction models are summarized in Table 4.2 and comparisons with the other models show how accurately these conduction mechanisms are fitted. It is reported that the change in the conduction mechanism of dielectric film is due

to the change in physical or chemical properties in the film. [23,24] Thus, the variation in conduction mechanism extracted from J-E characteristics among samples is due to differences in oxygen binding state, composition, and trap density of the film. In order to investigate the cause of the change in electrical characteristics, I analyzed the chemical properties of AlO_x thin film under various conditions and the electrical performance when applied to TFTs as a dielectric layer.

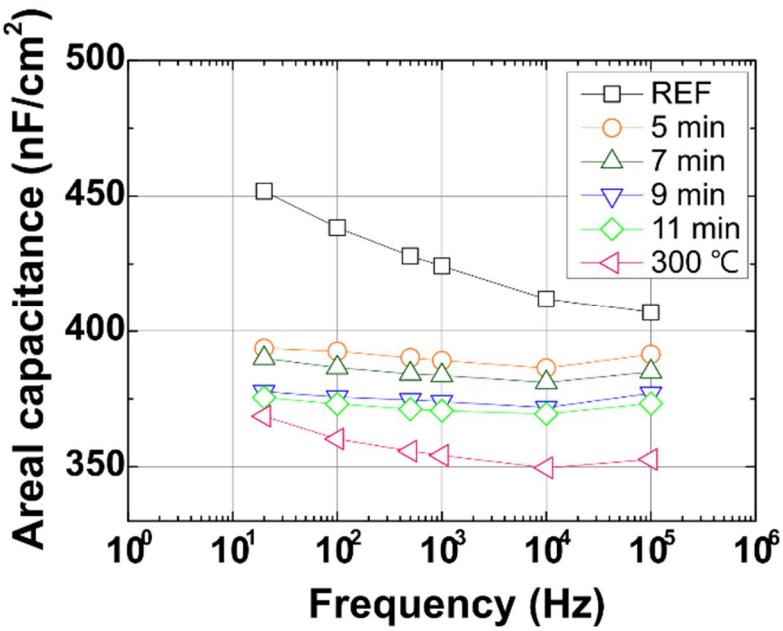

Figure 3. 2 Frequency versus areal capacitance of AlO_x thin film with various APP treatment condition and annealing temperature.

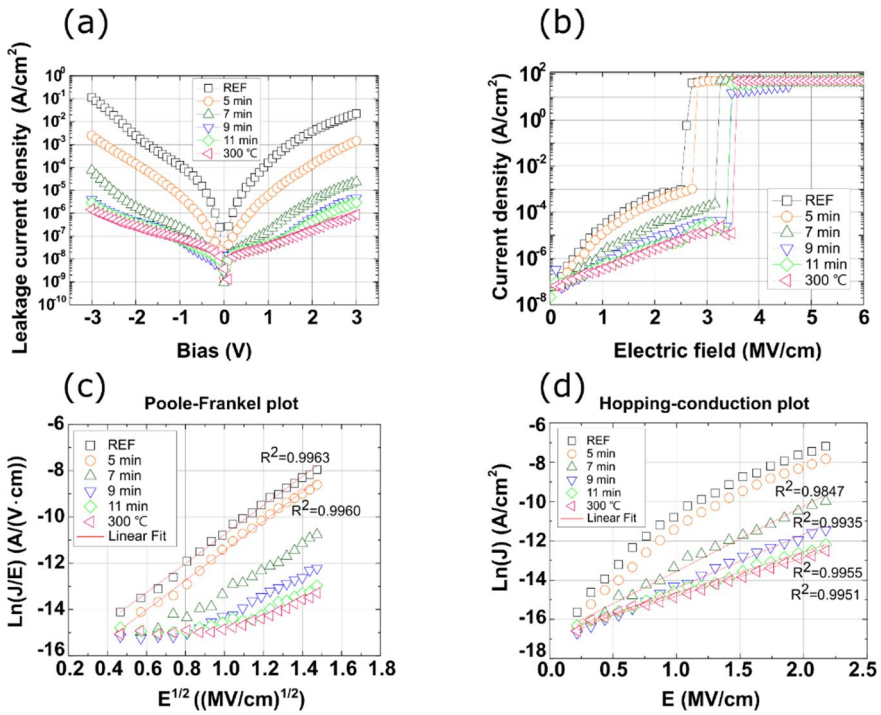

Figure 3. 3 Bias versus leakage current density (a) and J-E characteristic (b) of AlO_x thin films. Ln(J/E)-$E^{1/2}$ plot (c) and Ln(J)-E plot (d) show a change in the conduction mechanism of AlO_x thin film with increasing the APP treatment time.

APP treatment		-	5 min	7 min	9 min	11 min	-
Annealing temperature (°C)		250 (REF)	250	250	250	250	300
Capacitance ($nF\ cm^{-2}$)	20 Hz	451.8	393.6	389.9	377.6	375.5	368.6
	100 Hz	438.4	392.5	386.5	375.7	373.2	360.2
	500 Hz	428.0	390.1	384.2	374.6	371.2	355.7
	1 kHz	424.3	389.1	383.6	373.9	370.7	354.2
	10 kHz	412.0	386.3	381.1	371.8	369.5	349.6
	100 kHz	407.1	391.4	384.9	377.1	373.3	352.7

Table 3. 1 The areal capacitance of AlO_x thin films with various fabrication conditions.

APP treatment	-	5 min	7 min	9 min	11 min	-
Annealing temperature (℃)	250 (REF)	250	250	250	250	300
Poole-Frenkel	**0.9963**	**0.9960**	0.9728	0.9396	0.7967	0.8139
Hopping-conduction	0.9568	0.9608	0.9874	**0.9935**	**0.9955**	**0.9951**
SCLC	0.9893	0.9862	0.9552	0.9394	0.9184	0.9228
F-N tunneling	0.7365	0.7168	0.4001	0.1054	0.2735	0.4344
Direct tunneling	0.7416	0.7403	0.7095	0.7790	0.7931	0.7982

Table 3. 2 The coefficient of determination in statistics, R^2 values for various conduction mechanism models. The closer R^2 value to 1, the more the conformity. (R^2 values greater than 0.9935 are shown in bold font)

3.4 Chemical structures of the AlO_x thin films

To analyze the chemical properties of the AlO_x thin films, XPS measurements was performed. Figure 3.4(a)-(f) show the O 1s spectrum of the AlO_x thin film with varying the APP treatment time. The O 1s spectrum of the AlO_x dielectric film can be deconvoluted into two peaks centered at 531.7 eV and 530.3 eV corresponding to OH^- and O^{2-}, respectively. [25] The measured data (open circles) was fitted by the Gaussian-Lorentzian function (solid line). Generally, aluminum (III) nitrate precursors form hexa-aqua metal complexes of $[Al(OH_2)_6]^{3+}$ and convert into the metal-oxide-metal frameworks through dehydroxylation and dehydration. [16,26] Consequently, it can be seen that the APP treatment reduces the OH^- intensity and increases the O^{2-} intensity, which can be considered as a contribution of the APP treatment to the formation of the metal-oxide-metal frameworks with elimination of the hydroxyl groups. (Figure 3.4(g)) Furthermore, as the APP time increases, the decreased intensity of the OH^- may be ascribed to the conversion of more aluminum hydroxides to form aluminum oxides. Particularly, the peak intensity ratio of O^{2-} and OH^- treated with the APP for 9 and 11 minutes was similar to that of the sample annealed at 300 °C. These results mean that the AlO_x thin film with chemical structure comparable to that annealed at high temperature can be obtained even at a low temperature process through the APP treatment.

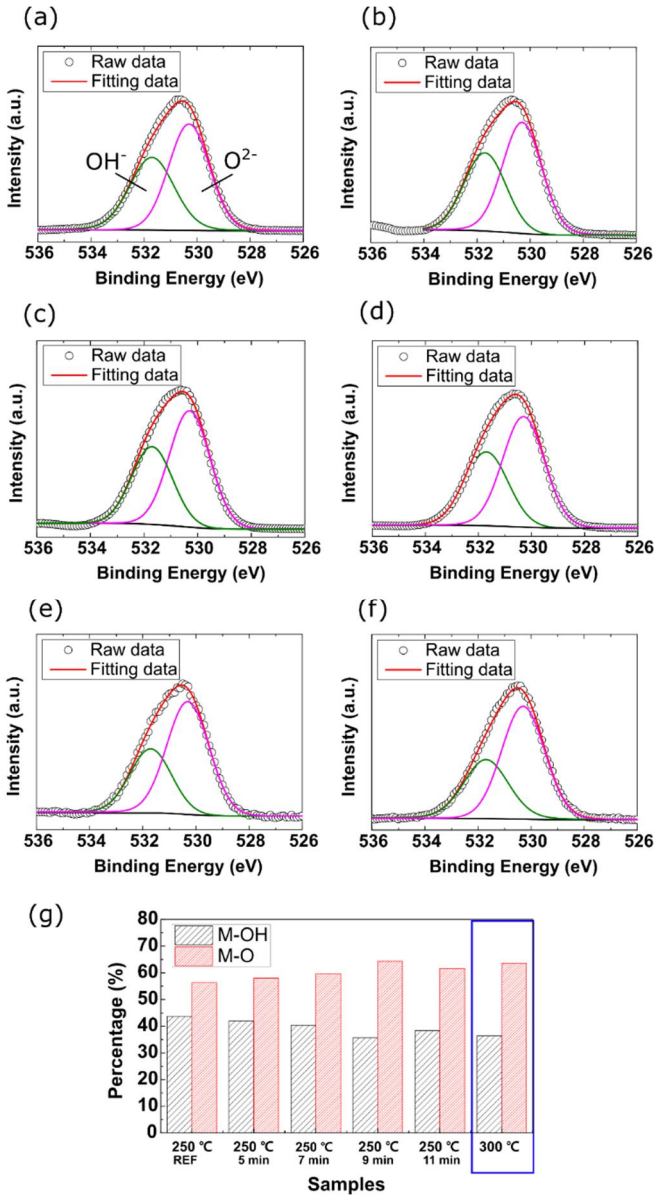

Figure 3. 4 The O 1s XPS spectra of AlO_x thin films at different annealing temperatures and APP treatment times of (a) 250 ℃- untreated, (b) 250 ℃- 5 minutes, (c) 250 ℃- 7 minutes, (d) 250 ℃- 9 minutes, (e) 250 ℃- 11 minutes, and (f) 300 ℃- untreated. (g) Percentage of M-OH and M-O bond of AlO_x thin films with various conditions.

3.5 Electrical performance of InO_x TFTs based on the APP treated AlO_x dielectric thin films

To verify the electrical characteristic of the TFTs according to the APP treatment time of the AlO_x dielectric films, I fabricated a conventional bottom gate TFT as shown in Figure 3.5(e). The transfer measurement was performed with a small range of gate-source voltage (V_G) sweep from -1 to 4 V at a drain voltage (V_D) of 1 V, which is good for low power consumption. Actually, in the TFT transfer characteristics, the physical parameters such as field-effect mobility and subthreshold swing (*SS*) were prominently changed according to the changes in APP treatment time. (Figure 3.6(a)) The field- effect mobility (μ) in the linear region was evaluated from the trans-conductance (g_m) as follows [1,27]:

$$g_m = \frac{\partial I_D}{\partial V_G}\Big|_{V_D} \ , \ \mu = \frac{L}{W} \frac{g_m}{C_{ox} V_D}$$

where W and L are constants representing the channel width and length, respectively, and C_{ox} is the gate capacitance per unit area. The APP-treated TFTs are shown as a field-effect mobility of 13.12 $cm^2 V^{-1} s^{-1}$ for 5 minutes, 16.91 $cm^2 V^{-1} s^{-1}$ for 7 minutes, 26.79 $cm^2 V^{-1} s^{-1}$ for 9 minutes, and and 26.38 $cm^2 V^{-1} s^{-1}$ for 11 minutes. Compared with the untreated AlO_x TFTs (REF) with field-effect

mobility of 9.77 cm^2 V^{-1} s^{-1}, the APP-treated AlO_x TFTs represent the significantly enhanced field-effect mobility. Also, the field-effect mobility of the sample treated with the APP for 9 and 11 minutes after annealing at 250 ℃ was close to that of the sample annealed at 300 ℃. Figure 3.6(b) shows the variation of the field-effect mobility according to the frequency change of capacitance measurement. It can be seen that the mobility variation of the TFT with the untreated AlO_x layer is changed to 3.04% according to the frequency change, but the mobility variation of the TFT with the APP-treated AlO_x layer is changed within 1.39%.

In addition, the *SS* value decreased monotonically as the APP treatment time of the AlO_x layer increased to 9 minutes and saturated hereafter. In the TFT with the untreated AlO_x layer (REF), the *SS* value was found to be 0.225 V/dec, but it was improved to 0.150 and 0.151 V/dec for TFTs with the APP treated for 9 and 11 minutes, respectively. The *SS* value is closely related to the trap located in interface or bulk between the dielectric and the semiconductor layer. Therefore, the maximum trapped charge density (N_{max}) can be extracted from the *SS* values using the following relationship [28]:

$$N_{max} = \left[\frac{SSlog(e)}{kT/q} - 1\right] \times \frac{C_{ox}}{q}$$

where k is the Boltzmann's constant, T is the absolute temperature, q is the

electronic charge. The lower value of N_{max} was obtained at 9 minutes- and 11 minutes-APP treated device. N_{max} values were found to be 7.4 x 10^{12} cm^{-2} eV^{-1} in REF device and 4.0x10^{12} and 4.1x10^{12} cm^{-2} eV^{-1} after the 9- and 11- minutes APP treatment, respectively. Generally, the lower value of N_{max} can be obtained at the smoother surface roughness because the smoother surface reduced the scattering effect at interface region. However, as aforementioned, the variation of the surface roughness according to the APP treatment time is very small (0.12~0.16 nm). Therefore, it is reasonable to ascribe the reduced N_{max} to the improvement of dielectric properties as well as the decreasing of interface trap density induced by the APP treatment. These results are in a good agreement with the tendency of the capacitance, the leakage current density, and oxygen binding state of the AlO_x dielectric film. The statistical values of the physical parameters extracted from the current-voltage characteristics are summarized in Table 4.3.

Actually, the properties of thin films deposited by the vacuum process do not change significantly when treated with the APP. On the other hand, our study shows that the properties of solution-processed dielectric films can be improved by the APP treatment. It can be assumed that the APP treatment changed the properties of the solution-processed thin films because the density of that is relatively low. For these assumptions, further research is ongoing depending on the type of process.

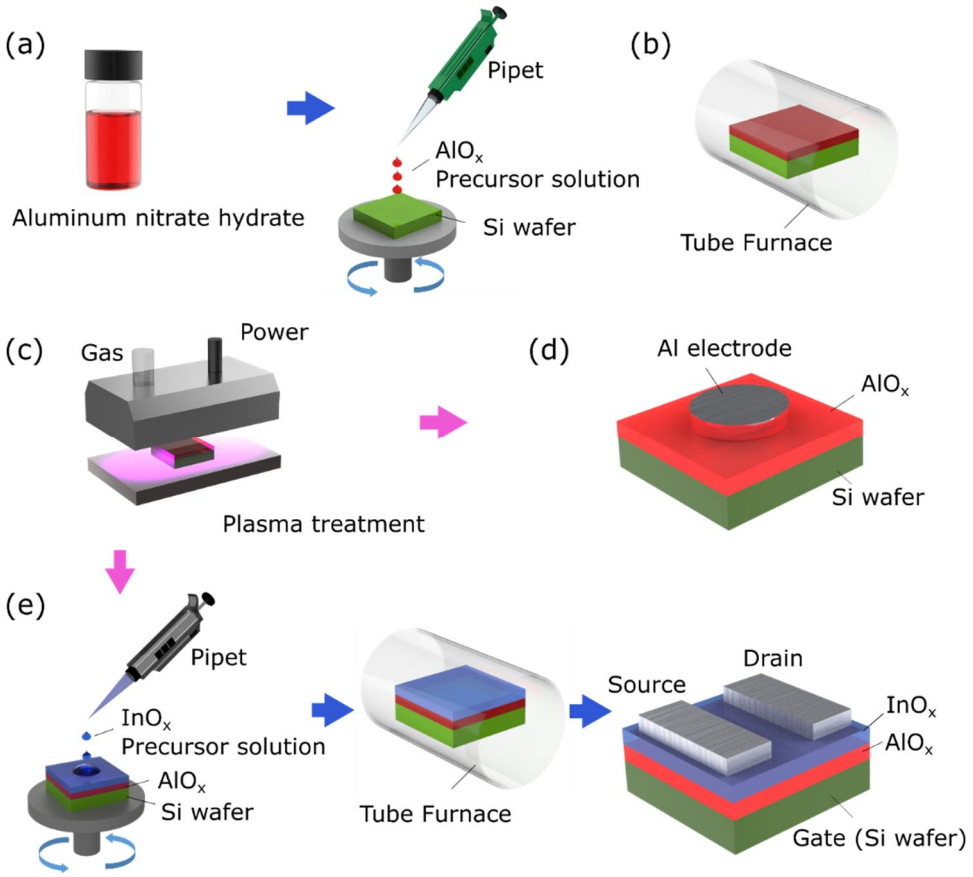

Figure 3. 5 Schematics of experimental procedures. (a) Spin-coating of AlO_x. (b) Thermal annealing into a tube furnace. (c) Atmospheric-pressure plasma treatment. (d) Thermally evaporated Al electrode. (e) TFT fabrication procedures.

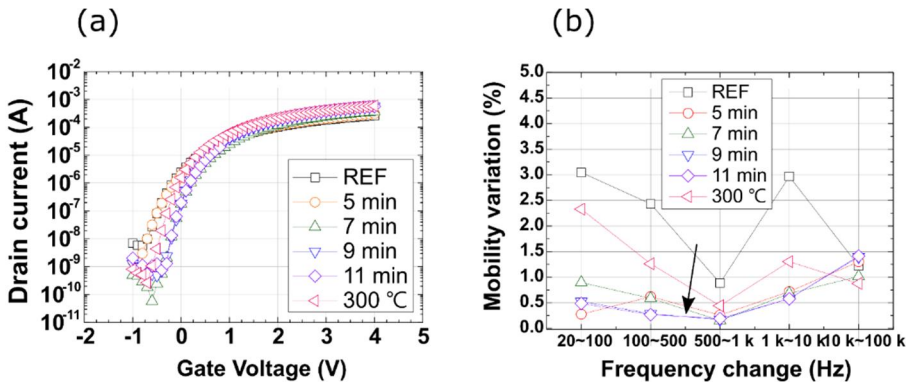

Figure 3. 6 Transfer characteristic curves (a) and frequency change versus field-effect mobility variation (b) of TFTs using AlO_x thin films with various APP treatment conditions annealed at 250 and 300 ℃.

APP treatment	-	**5 min**	**7 min**	**9 min**	**11 min**	-
Annealing temperature (°C)	250 (REF)	250	250	250	250	300
Field-effect mobility (cm^2/Vs) <σ>	9.77 <0.36>	13.12 <0.09>	16.91 <0.13>	26.79 <0.15>	26.38 <0.16>	27.76 <0.51>
On/off current ratio	$4.6x10^4$	$2.6x10^5$	$6.2x10^6$	$2.4x10^6$	$1.1x10^6$	$2.2x10^6$
Subthreshold swing (V/dec) <σ>	0.225 <0.007>	0.189 <0.006>	0.175 <0.007>	0.150 <0.009>	0.151 <0.007>	0.163 <0.008>
N_{max} ($cm^{-2}\,eV^{-1}$)	$7.4x10^{12}$	$5.8x10^{12}$	$5.17x10^{12}$	$4.0x10^{12}$	$4.1x10^{12}$	$4.6x10^{12}$

Table 3. 3 Summary of field-effect mobility, on/off current ratio, subthreshold swing, and N_{max} of AlO_x/ InO_x TFTs with different atmospheric-pressure plasma treatment time and annealing temperature in 30 samples by one-run.

3.6 Conclusion

In conclusion, I introduce the APP treatment technique that can simply improve the electrical performance of solution-processed dielectric films without additional annealing temperature rise or vacuum equipment. Through the APP treatment, the AlO_x dielectric films exhibited a low leakage current and a constant capacitance value over the whole frequency operating range, confirming that this is due to the conversion of more aluminum hydroxides to form aluminum oxides. It is also verified that the conduction mechanism of leakage current changes at the sample treated with the APP for 9 minutes. Finally, when fabricated with TFTs, the field-effect mobility was improved from 9.77 $cm^2 V^{-1} s^{-1}$ to 26.79 $cm^2 V^{-1} s^{-1}$, similar to 27.76 $cm^2 V^{-1} s^{-1}$ of the sample annealed at 300 ℃. These results reported here imply that the APP technique can provide advances in industries that require low temperature processes, such as flexible devices and roll-to-roll processing because it can simply and effectively fabricate high-quality solution-processed dielectric films at low temperature.

3.7 Experimental details

Precursor solution synthesis. Heavily boron-doped Si wafers used as substrates were sequentially cleaned in detergent, distilled water, acetone, and isopropyl alcohol. Afterwards, UV-ozone treatment was carried out to increase the hydrophilicity of the surface. AlO_x precursor solution (0.2 M) was prepared by dissolving aluminum nitrate hydrate (Sigma-Aldrich 99.997% trace metals basis) in 10 mL of 18.2 MΩ deionized water, and then the solution was stirred vigorously for 3 days at 25 °C. In addition, to evaluate the characteristics of the TFTs to which the AlO_x dielectric film is applied, InO_x precursor solution (0.15 M) was prepared by dissolving indium nitrate hydrate (Sigma-Aldrich 99.999% trace metals basis) in deionized water.

Film fabrication and the APP treatment. The AlO_x precursor solution was filtered through a 0.22 mm syringe filter PTFE (DISMIC 13HP020AN, Advantec, Japan), and was spin-coated onto substrates at a speed of 2000 rpm for 30 seconds under a humidity of 35%. Then the films were soft-baked at 250 °C for 60 seconds, and were hard-baked in a tube furnace under <10% humidity at 250 °C for 4 hours. Afterwards, the films were treated using an atmospheric-pressure plasma equipment (Multi-Layer Electrode, PSM Inc.) [14]. Nitrogen and compressed dry air were used to generate the plasma. The distance between the plasma source and sample was 5 mm. Schematics of

experimental procedures are shown in Figure 3.5. The surface morphologies of AlO_x dielectric films were observed by atomic force microscopy (AFM) (XE150, PSIA Inc.). X-ray photoelectron spectroscopy (XPS) (SIGMA PROBE, ThermoVG) was used to obtain the electronic state of the AlO_x films.

Fabrication of the MIM and TFT devices. To measure the capacitance and leakage current of AlO_x dielectric thin film, cylindrical aluminum electrodes with a radius of 250 μm and a thickness of 100 nm were deposited by thermal evaporation. For the TFT, InO_x precursor solution coated onto the AlO_x film at a speed of 5000 rpm for 30 seconds under a humidity of 10% and annealing at 250 ℃ for 4 hours. Thicknesses of AlO_x and InO_x thin films were 13.6 and 6.4 nm, respectively. Then, the aluminum source drain electrodes with channel width of 1000 μm and length of 50 μm were deposited on InO_x film by thermal evaporation using a shadow mask. Subsequently, the InO_x layer was patterned by the conventional photolithography method (Figure 3.5 and 3.7).

Measurement of the electrical characteristics. Electrical characteristics of all devices were measured in a dark and atmospheric condition using Agilent Technologies 4284A precision LCR meter and 4155B semiconductor parameter analyzer.

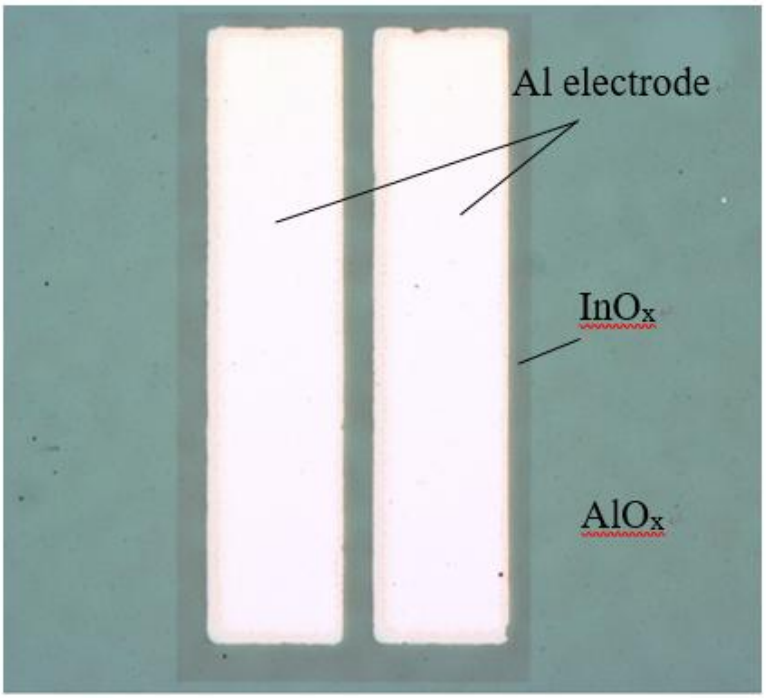

Figure 3. 7 Optical microscope image of patterned InO_x TFT with AlO_x

3.8 References

[1] E. Fortunato, P. Barquinha, and R. Martins, Adv. Mater. **24**, 2945 (2012).

[2] K.-H. Lim, K. Kim, S. Kim, S.Y. Park, H. Kim, and Y.S. Kim, Adv. Mater. **25**, 2994 (2013).

[3] R. Chen and L. Lan, Nanotechnology **30**, 312001 (2019).

[4] Y. Hwan Hwang, J.-S. Seo, J. Moon Yun, H. Park, S. Yang, S.-H. Ko Park, and B.-S. Bae, NPG Asia Mater. **5**, e45 (2013).

[5] K.-H. Lim, J. Lee, J.-E. Huh, J. Park, J.-H. Lee, S.-E. Lee, and Y.S. Kim, J. Mater. Chem. C **5**, 7768 (2017).

[6] J.H. Park, K. Kim, Y.B. Yoo, S.Y. Park, K.-H. Lim, K.H. Lee, H.K. Baik, and Y.S. Kim, J. Mater. Chem. C **1**, 7166 (2013).

[7] B.N. Pal, B.M. Dhar, K.C. See, and H.E. Katz, Nat. Mater. **8**, 898 (2009).

[8] J. Robertson, Reports Prog. Phys. **69**, 327 (2006).

[9] G. Adamopoulos, S. Thomas, P.H. Wöbkenberg, D.D.C. Bradley, M.A. McLachlan, and T.D. Anthopoulos, Adv. Mater. **23**, 1894 (2011).

[10] P.N. Plassmeyer, G. Mitchson, K.N. Woods, D.C. Johnson, and C.J. Page, Chem. Mater. **29**, 2921 (2017).

[11] K.H. Lim, J.E. Huh, J. Lee, N.K. Cho, J.W. Park, B. Il Nam, E. Lee, and Y.S. Kim, ACS Appl. Mater. Interfaces **9**, 548 (2017)

[12] L. Keun Ho, H. Sun Woong, P. Jee Ho, Y. Young Bum, L. Se Jong, B. Hong Koo, and S. Kie Moon, Jpn. J. Appl. Phys. **55**, 10304 (2016).

[13] S.J. Heo, D.H. Yoon, T.S. Jung, and H.J. Kim, J. Inf. Disp. **14**, 79 (2013).

[14] J. Park, J.E. Huh, S.E. Lee, J. Lee, W.H. Lee, K.H. Lim, and Y.S. Kim, ACS Appl. Mater. Interfaces **10**, 30581 (2018).

[15] I. Isakov, H. Faber, M. Grell, G. Wyatt-Moon, N. Pliatsikas, T. Kehagias, G.P. Dimitrakopulos, P.P. Patsalas, R. Li, and T.D. Anthopoulos, Adv. Funct. Mater. **27**, 1 (2017).

[16] J.H. Cho, J. Lee, Y. Xia, B. Kim, Y. He, M.J. Renn, T.P. Lodge, and C. Daniel Frisbie, Nat. Mater. **7**, 900 (2008).

[17] J. Zhuang, Q.J. Sun, Y. Zhou, S.T. Han, L. Zhou, Y. Yan, H. Peng, S. Venkatesh, W. Wu, R.K.Y. Li, and V.A.L. Roy, ACS Appl. Mater. Interfaces **8**, 31128 (2016).

[18] W. Xu, H. Wang, L. Ye, and J. Xu, J. Mater. Chem. C **2**, 5389 (2014).

[19] W. Xu, H. Wang, F. Xie, J. Chen, H. Cao, and J. Bin Xu, ACS Appl. Mater. Interfaces **7**, 5803 (2015).

[20] J.H. Park, Y.B. Yoo, K.H. Lee, W.S. Jang, J.Y. Oh, S.S. Chae, H.W. Lee, S.W. Han, and H.K. Baik, ACS Appl. Mater. Interfaces **5**, 8067 (2013).

[21] F.C. Chiu, Adv. Mater. Sci. Eng. **2014**, (2014).

[22] B. Il Nam, J.S. Park, K.H. Lim, Y.K. Ahn, J. Lee, J.W. Park, N.K. Cho, D. Lee, H.B.R. Lee, and Y.S. Kim, Appl. Phys. Lett. **111**, (2017).

[23] A. Hasegawa, T. Tanno, S. Nogami, and M. Satou, J. Nucl. Mater. **417**, 491 (2011).

[24] J.E. Huh, J. Park, J. Lee, S.E. Lee, J. Lee, K.H. Lim, and Y.S. Kim, J. Ind. Eng. Chem. **68**, 117 (2018).

[25] J. Van den Brand, W.G. Sloof, H. Terryn, and J.H.W. De Wit, Surf. Interface Anal. **36**, 81 (2004).

[26] Y.S. Rim, H. Chen, T. Bin Song, S.H. Bae, and Y. Yang, Chem. Mater. **27**, 5808 (2015).

[27] D.K. Schroder, *Semiconductor Material and Device Characterization: Third Edition* (2005).

[28] M. McDowell, I.G. Hill, J.E. McDermott, S.L. Bernasek, and J. Schwartz, Appl. Phys. Lett. **88**, 2004 (2006).

Chapter 4

Conclusion

I present an atmospheric-pressure plasma (APP) treatment technique for improving the electrical performance of solution-processed films. Firstly, I have implemented improvements in important TFT parameters, V_{on} and the on/off current ratio, which still keep up the high field-effect mobility, by introducing the APP treatment into solution-processed InO_x TFTs. Secondly, AlO_x dielectric film using aqueous route method was deposited by a solution process and its characteristics were improved. Characteristic changes through APP treatment were observed by measurement of capacitance-frequency and breakdown voltage. It was observed that the breakdown voltage of AlO_x thin film was increased by APP treatment. To investigate the changes of binding relationship according to APP treatment time, X-ray photoelectron spectroscopy (XPS) was performed. TFTs were fabricated by depositing a solution-processed InO_x with a semiconductor film, and the characteristics were evaluated. The field-effect mobility was increased compared to the untreated samples. Thin-film deposition including semiconductor and gate dielectric and plasma treatment were performed in a non-vacuum environment. The process temperature was below 250 ℃.

In summary, I introduce the potential of APP treatment that can simply control the carrier concentration of solution-processed OS thin film and improve the breakdown voltage of solution-processed gate dielectric thin film. This APP technique can provide advances toward industrial applications of solution-

processed TFTs, while maintaining the advantages of the solution process.

List of publications

-. **Jintaek Park**, Jae Eun Huh, Sung Eun Lee, Junhee Lee, Won Hyung Lee, Keon Hee Lim, and Youn Sang Kim. "Effective Atmospheric-Pressure Plasma Treatment toward High-Performance Solution-Processed Oxide Thin-Film Transistors." *ACS Applied Materials and Interfaces* 10, no. 36, 2018

-. **Jintaek Park**[*], Nam-Kwang Cho[*], Sung-Eun Lee, Eun Goo Lee, Junhee Lee, Changik Im, Hyunjae Na, and Youn Sang Kim. "Atmospheric-Pressure Plasma Treatment toward High-Quality Solution-Processed Aluminum Oxide Gate Dielectric Films in Thin-Film Transistors." *Nanotechnology*, 2019.

-. Nam-Kwang Cho[*], **Jintaek Park**[*], Donggun Lee, Jun-Woo Park, Won Hyung Lee, and Youn Sang Kim. "Investigation of Vertical Current Phenomena in the Insulator/Oxide Semiconductor Heterojunction Using XPS Analysis and an Atmospheric-Pressure Plasma Treatment System." *ACS Applied Electronic Materials* 1, no. 8, 2019

-. Jae Eun Huh, **Jintaek Park**, Junhee Lee, Sung Eun Lee, Jinwon Lee, Keon Hee Lim, and Youn Sang Kim. "Effects of Process Variables on Aqueous-Based AlO x Insulators for High-Performance Solution-Processed Oxide Thin-Film Transistors." *Journal of Industrial and Engineering Chemistry* 68, 2018

-. Eun Goo Lee, **Jintaek Park**, Sung-Eun Lee, Junhee Lee, Changik Im, Gayeong Yoo, Jeeyoung Yoo, and Youn Sang Kim. "Superconcentrated Aqueous

Electrolyte and UV Curable Polymer Composite as Gate Dielectric for High-Performance Oxide Semiconductor Thin-Film Transistors." *Applied Physics Letters* 114, no. 17, 2019

-. Sung-Eun Lee, **Jintaek Park**, Junhee Lee, Eun Goo Lee, Changik Im, Hyunjae Na, Nam-Kwang Cho, Keon-Hee Lim, and Youn Sang Kim. "Surface-Functionalized Interfacial Self-Assembled Monolayers as Copper Electrode Diffusion Barriers for Oxide Semiconductor Thin-Film Transistor." *ACS Applied Electronic Materials* 1, no. 3, 2019

-. Junhee Lee, Jinwon Lee, **Jintaek Park**, Sung-Eun Lee, Eun Goo Lee, Changik Im, Keon-Hee Lim, and Youn Sang Kim. "Solution-Grown Homojunction Oxide Thin-Film Transistors." Research-article. *ACS Applied Materials & Interfaces* 11, 2019

-. Keon-Hee Lim, Jinwon Lee, Jae-Eun Huh, **Jintaek Park**, Jun-Hee Lee, Sung-Eun Lee, and Youn Sang Kim. "A Systematic Study on Effects of Precursors and Solvents for Optimization of Solution-Processed Oxide Semiconductor Thin-Film Transistors." *J. Mater. Chem. C*, 2017

- Hyun Jae Na, Nam Kwang Cho, **Jintaek Park**, Sung Eun Lee, Eun Goo Lee, Changik Im, and Youn Sang Kim. "A Visible Light Detector Based on a Heterojunction Phototransistor with a Highly Stable Inorganic CsPbI:XBr3-x Perovskite and In-Ga-Zn-O Semiconductor Double-Layer." *Journal of Materials Chemistry C* 7, no. 45, 2019

- Eun Goo Lee, **Jintaek Park**, Sung-eun Lee, Hyun-jae Na, Nam-kwang Cho, Changik Im, Yong Hyun Cho, and Youn Sang Kim. “Oxygen Radical Control via Atmospheric Pressure Plasma Treatment for Highly Stable IGZO Thin-Film Transistors,” *IEEE Transactions on Electron Devices* 2020 Early Access

요 약 (국문초록)

대기 플라즈마 처리를 통한 고성능 용액 공정 금속 산화물 박막 트랜지스터 개발에 관한 연구

박 진 택
융합과학부 나노융합전공
융합과학기술대학원
서울대학교

디스플레이는 많은 정보를 다양한 방법을 통해 효율적으로 전달받기 원하는 사람들의 요구를 충족시키기 위해, 고해상도 및 대형화 되어 왔다. 최근에는, 개인용 모바일 기기가 각광 받음에 따라 웨어러블이나 플렉서블 혹은 투명 디스플레이로 그 진화의 방향을 다르게 하고 있다. 이러한 미래 디스플레이를 개발하기 위해서는 디스플레이에서 스위칭 소자로서 핵심적인 역할을 하고 있는 박막 트랜지스터를 유연하고 투명하게 개발하는 것이 필수적이다.

현재 LCD 디스플레이에서 널리 사용되고 있는 비정질 실리콘 박막 트랜지스터는 불투명하고 이동도가 낮은 단점이 있다. 또한, 모바일 기기에 사용되는 LTPS (Low Temperature Poly Silicon) 박막 트랜지스터는 고이동도 특성은 가지지만, 불투명하고 전기적 특성의 불균일성으로

인해 대형화가 어렵다. 따라서, 투명하고 유연한 특성을 가지는 금속 산화물 박막 트랜지스터를 미래 디스플레이에 적용하기 위한 많은 연구가 진행되고 있다. 특히, 용액 공정으로 제작 된 금속 산화물 박막 트랜지스터는 복잡한 진공 장비를 사용하지 않고 대면적 생산 및 연속 공정으로 제조가 가능하기 때문에 많은 관심을 받아 왔지만, 전기적 특성이 진공 공정으로 제작 된 박막 트랜지스터에 비해 낮기 때문에 실제 산업의 적용에 문제점이 있다.

본 연구에서는 고성능 용액 공정 금속 산화물 박막 트랜지스터를 개발하기 위해 대기 플라즈마 처리 방법을 제안하였다. 첫번째로, 용액 공정으로 제작 된 InO_x 산화물 반도체를 대기 플라즈마 처리하여 박막 트랜지스터의 스위칭 소자로서 중요한 인자 인 turu-on voltage (V_{on}), on/off 전류 비 등의 전기적 특성을 조절하였다. 두번째로, AlO_x 박막을 박막 트랜지스터의 필수적인 구성 인자인 절연체로 적용하고, 대기 플라즈마 처리를 통해 특성 향상을 확인하였다. 이를 통해 전기적 특성이 향상 된 용액 공정 산화물 반도체 트랜지스터를 구현하였고, 이러한 현상들을 atomic force microscopy (AFM), X-ray photoelectron spectroscopy (XPS), UV-visible spectroscopy와 모델링 등의 분석을 통해 규명하였다.

결론으로, 본 연구에서는 대기 플라즈마 처리를 통해서 대기중에서 제작이 가능한 금속 산화물 박막 트랜지스터를 개발하였다. 이 방법을 통해 대기중에서 용액 공정의 장점을 유지하면서, 금속 산화물 반도체

와 절연체 박막의 전기적 특성을 향상시킬 수 있었다. 이러한 연구를 통하여 고해상도, 투명 및 플렉서블과 같은 미래 디스플레이에서 용액 공정 산화물 반도체를 구동 소자로서 적용하는데 있어 높은 가능성을 제시하였다.

주요어: 대기 플라즈마, 산화물 반도체, 절연체, 박막 트랜지스터, 용액 공정, 저온 공정

학 번: 2016-39007